REPORT DOCUMENTATION PAGE

1. AGENCY USE ONLY (Leave blank)	2. REPORT DATE	3. REPORT TYPE AND DATES COVERED
	05 January, 1998	Technical · 8/1/97 – 2/28/98

4. TITLE AND SUBTITLE

Preparation and Characterization of Dendrimer Monolayers and Dendrimer-Alkylthiol Mixed Monolayers adsorbed to Gold

5. FUNDING NUMBERS

N00014-93-11338
300x084yip
96PRO-1027

6. AUTHOR(S)

H. Tokuhisa, M. Zhao, L. Baker, V. Phan, D. Dermody
M. Gacia, R. Peez, R.M. Crooks

7. PERFORMING ORGANIZATION NAME(S) AND ADDRESS(ES)

Department of Chemistry
Texas A&M University
College Station, Texas 77843-3255

8. PERFORMING ORGANIZATION REPORT NUMBER

31

9. SPONSORING/MONITORING AGENCY NAME(S) AND ADDRESS(ES)

Office of Naval Research
800 North Quincy Street
Arlington, Virginia 22217-5000

10. SPONSORING/MONITORING AGENCY REPORT NUMBER

11. SUPPLEMENTARY NOTES

J. Am. Chem. Soc., submitted 12/16/97

DTIC QUALITY INSPECTED 2

12b. DISTRIBUTION CODE

13. ABSTRACT (Maximum 200 words)

Single-component monolayers of dendrimers and two-component monolayers consisting of dendrimers and n-alkylthiols immobilized on Au substrates are described. single-component monolayers are prepared by exposing an Au substrate to ethanolic solutions of amine- or hydroxy-terminated polyamidoamine (PAMAM) dendrimers. The resulting monolayers are highly stable and nearly close-packed for dendrimer generations ranging from 4 to 8 (G4-G8), Electrochemical ac-impedance measurements indicate that the dendrimer surface is very porous towards the electroactive redox couple $Fe(CN)_6^{3-/4-}$. Ferrocene-terminated dendrimer monolayers have also been investigated. Exposure of higher-generation dendrimer monolayers to ethanolic solutions of hexadecylthiol (C16SH) results in a dramatic compression of the dendrimers, and caused them to reorient on the surface from an oblate to prolate configuration. The dendrimers originally present on the surface do not desorb as a consequence of this configurational change. Comparison of the extent of adsorption of C16SH in different media (vapor-phase N_2, hexane, and ethanol) shows that solvation of the dendrimer endgroups is the primary driving force for the structural change. Finally, the reactivity and stability of the dendrimer monolayers is investigated by on-surface functionalization of the dendrimer monolayer with 4-(trifluoromethyl) benzoyl chloride. The physical and chemical properties of the single- and two-component monolayers are evaluated using reflection infrared spectroscopy, ellipsometry, contact-angle measurements, ac-impedance spectroscopy, cyclic voltammetry, and surface acoustic wave (SAW)-based analyte-dosing experiments.

14. SUBJECT TERMS

15. NUMBER OF PAGES 45

16. PRICE CODE

17. SECURITY CLASSIFICATION OF REPORT	18. SECURITY CLASSIFICATION OF THIS PAGE	19. SECURITY CLASSIFICATION OF ABSTRACT	20. LIMITATION OF ABSTRACT
Unclassified	Unclassified	Unclassified	

Preparation and Characterization of Dendrimer Monolayers and Dendrimer-Alkylthiol Mixed Monolayers Adsorbed to Gold

Hideo Tokuhisa, Mingqi Zhao, Lane A. Baker, Vy T. Phan, Daniel L. Dermody, Maurie E. Garcia, Robert F. Peez, and Richard M. Crooks[*][1]

<u>Department of Chemistry</u>

<u>Texas A&M University</u>

<u>P. O. Box 300012</u>

<u>College Station, TX 77842-3012</u>

Thomas M. Mayer

<u>Surface and Interface Science Department</u>

<u>Sandia National Laboratories</u>

<u>Albuquerque, NM 87185-1413</u>

[1]E-Mail: crooks@chemvx.tamu.edu, Voice: 409-845-5629, Fax: 409-845-1399

[*]Author to whom correspondence should be addressed

Abstract

Single-component monolayers of dendrimers and two-component monolayers consisting of dendrimers and n-alkylthiols immobilized on Au substrates are described. Single-component monolayers are prepared by exposing an Au substrate to ethanolic solutions of amine- or hydroxy-terminated polyamidoamine (PAMAM) dendrimers. The resulting monolayers are highly stable and nearly close-packed for dendrimer generations ranging from 4 to 8 (G4-G8). Electrochemical ac-impedance measurements indicate that the dendrimer surface is very porous towards the electroactive redox couple $Fe(CN)_6^{3-/4-}$. Ferrocene-terminated dendrimer monolayers have also been investigated. Exposure of higher-generation dendrimer monolayers to ethanolic solutions of hexadecylthiol (C16SH) results in a dramatic compression of the dendrimers, and causes them to reorient on the surface from an oblate to prolate configuration. The dendrimers originally present on the surface do not desorb as a consequence of this configurational change. Comparison of the extent of adsorption of C16SH in different media (vapor-phase N_2, hexane, and ethanol) shows that solvation of the dendrimer endgroups is the primary driving force for the structural change. Finally, the reactivity and stability of the dendrimer monolayers is investigated by on-surface functionalization of the dendrimer monolayer with 4-(trifluoromethyl)benzoyl chloride. The physical and chemical properties of the single- and two-component monolayers are evaluated using reflection infrared spectroscopy, ellipsometry, contact-angle measurements, ac-impedance spectroscopy, cyclic

voltammetry, and surface acoustic wave (SAW)-based analyte-dosing

experiments.

Introduction

Here, we describe monolayers prepared by the direct adsorption of several kinds of dendrimers onto Au substrates. In some cases the monolayers are nearly close-packed and in most cases are very strongly adsorbed to the Au surface. We also discuss the novel structural and chemical properties of mixed monolayers prepared from n-alkylthiols and dendrimers (Scheme 1). The dendrimer monolayers have several important properties. First, the higher generation dendrimers yield quasi-three-dimensional surfaces characterized by a much higher density of functional groups than found on linear, alkyl-based self-assembled monolayers (SAMs).[1-3] Second, the terminal groups on the dendrimers can be post-functionalized without loss of dendrimers from the surface, which greatly expands their versatility. Third, composite monolayers with properties that are not a linear combination of the individual components can be prepared. We believe the simplicity and unique properties of directly adsorbed dendrimer monolayers will lead to their use in many technological applications including chemical sensors,[4,5] adhesion,[6] and membrane chemistry.

Scheme 1

SAMs[1-3,7] on metal, semiconductor, and insulating substrates have been studied extensively for use in a wide range of potential applications, including corrosion passivation,[8,9] bio- and chemical

sensors,[10,11] wetting,[12] and lithography.[13,14] The current broad
interest in SAMs arises from the simplicity of their preparation
and the reproducibility and predictability of their physical and
chemical properties. Specifically, their ability to form ordered,
densely packed layers, with reactive and easily modified terminal
groups make SAMs an ideal platform for both fundamental studies
and applied technologies. However, for some applications SAMs
prepared from molecules dominated by simple alkyl chains have some
significant disadvantages. First, they yield strictly two-
dimensional surfaces, which may not be optimal for certain
applications. For example, the steric crowding of the terminal
groups of planar SAMs often results in low monolayer reactivity.
Additionally, for applications such as chemical sensing or
adhesion, the relatively low density of reactive groups per unit
area available from planar SAMs may not be optimal. Second,
depending on the type of surface-linking chemistry, planar SAMs,
which are usually monopodal, may be of limited stability.[15-20]
Clearly there is a need to increase the dimensionality of SAMs to
enhance their functional group density and to improve their
substrate adhesion and stability. The dendrimer SAMs discussed
here achieve these objectives. Alternative strategies based on
immobilization of linear polymers can also be used to address
these goals, but the inherent flexibility of these materials makes
molecular-level manipulation and self organization difficult.[21-24]

Dendritic polymers (dendrimers)[25-27] possess a well-defined
globular structure characterized by three distinct structural
features: a central core, repetitive branching units, and terminal

groups. This simple and distinct framework provides a structure that is molecularly controllable based on the type of core, the amount and type of branching, and the functionality of the end groups. For example, the number of terminal groups increases exponentially as a function of dendrimer size or generation: a fourth generation (G4) dendrimer has 64 terminal groups and this number increases to 1024 for G8. Due to the unique chemical and structural properties of dendrimers, a number of potential applications have been proposed. These include catalysis,[28] encapsulation and controlled release,[29] chemical sensors,[4,5] and biomimetic materials.[30]

Besides the covalent SAM-linking approach developed in our laboratory and described previously,[4,5] a variety of other strategies have been developed for attaching dendrimers to surfaces. For example, redox-active ferrocenyl dendrimers have been electrochemically deposited onto a Pt electrode.[31,32] An amine-terminated dendrimer has been immobilized onto an amine-functionalized silicon surface via complexation with Pt^{2+}.[33] It has also been found that protonation of amine-terminated dendrimers leads to adsorption on a hydrophilic silicon oxide surface.[34] Finally, Langmuir films of polyether-based dendrimers have been investigated.[35] Compared to these approaches, the strategy described here is simple and versatile, and therefore has excellent potential for technological applications.

Experimental Section

Substrates. Au-coated substrates were prepared by electron-beam deposition of 10 nm of Ti followed by 200 nm of Au onto Si(100) wafers (Lance Goddard Associates, Foster City, CA).[36] Au-coated SAW devices were prepared in a same manner on polished ST-cut quartz. Before each experiment all wafers and devices were cleaned in a low-energy Ar plasma cleaner at medium power for 1 min (Harrick Scientific Corporation, NY, model PDC-32G).

Chemicals and solutions. Amine- and hydroxy-terminated polyamidoamine dendrimers (Starburst[TM] (PAMAM) Dendrimers, G0, G2, G4, G8, Dendritech, Inc., Midland, MI) were used as received. Fifth-generation, amine-terminated poly(iminopropane-1,3-diyl) dendrimers, 64-Cascade:1,4-Diaminobutane[4]:(1-azabutylidene)[60]:propylamine, (DAB(PA)$_{64}$, DSM Fine Chemicals, The Netherlands), were used as precursors for the ferrocene-terminated dendrimers (D-Fc) after drying in vacuo. $CH_3(CH_2)_4SH$ (Aldrich 98%), $CH_3(CH_2)_6SH$ (Aldrich 90%), and $CH_3(CH_2)_{15}SH$ (Aldrich 98%) were distilled once under reduced pressure prior to use. Ferrocenecarboxylic acid (Aldrich 97%), oxalyl chloride (Aldrich 98%), chlorobenzene (Aldrich 99.5%), n-heptane (Aldrich 99+%), benzene (Aldrich 99.9%), carbon tetrachloride (Aldrich 99.9%), acetone (EM science 99.5%), 1-butanol (Aldrich 99.8%), $Ru(NH_3)_6Cl_3$ (Strem Chemicals), and $K_4Fe(CN)_6$ and $K_3Fe(CN)_6$ (Fisher Scientific) were all used as received.

Unless otherwise noted, electrochemical data were obtained in a buffered electrolyte solution consisting of 0.5 M Na_2SO_4 and

0.025 M KH_2PO_4 + 0.025 M Na_2HPO_4 (pH = 6.3). All aqueous solutions were prepared using 18 MΩ·cm deionized water (Millipore).

Immediately preceding electrochemical experiments solutions were deoxygenated with N_2. During ac-impedance experiments the solutions were purged with N_2 at the rate of about two bubbles per second, and during cyclic voltammetry experiments N_2 was gently blown over the solution. All of these experiments were carried out at 22±2 °C.

Procedures. The amine- and hydroxy-terminated PAMAM dendrimer surfaces were prepared by immersing a plasma-cleaned Au surface in an ethanolic solution of the dendrimer at 22±2 °C (unless stated otherwise) for 15-20 h. The concentration based on the number of primary amine terminal groups was always 6.4 mM, which corresponds to absolute dendrimer concentrations of: G0, 1.6 mM; G2, 0.40 mM; G4, 0.10 mM; G8, 0.063 mM. Dendrimer deposition was followed by copious rinses with ethanol and water, and drying with N_2. DAB(PA)$_{64}$ ferrocene-terminated dendrimers (D-Fc) were prepared as previously described by Cuadrado et al.[37] Satisfactory ^{1}H-NMR spectra were obtained and the integrated intensity of the ferrocene-related peaks was compared to that of the internal methylene peaks. The average degree of functionalization was found to be 70%. Modification of Au substrates with D-Fc was identical to the procedure described for the PAMAM dendrimers except 0.01 mM chloroform solutions of D-Fc were used.

Mixed monolayers consisting of PAMAM dendrimers and

8

$CH_3(CH_2)_{15}SH$ (C16SH) were prepared by either immersing the dendrimer-modified Au substrate in a 1 mM ethanolic or hexane solution of C16SH, or by immersing a naked Au surface in an ethanolic solution containing both C16SH and dendrimer for 15-20 h. C16SH vapor dosing of dendrimer-modified surfaces was performed by passing a C16SH-saturated N_2 vapor over the substrate at 40 °C in a glass vessel for 3 h.

Characterization. As described previously,[38] FTIR-external reflection spectroscopy (FTIR-ERS) measurements were made using a Digilab FTS-40 spectrometer equipped with a Harrick Scientific Seagull reflection accessory and a liquid-N_2-cooled MCT detector. All spectra were the sum of 256 or fewer individual scans using p-polarized light at an 84° angle of incidence with respect to the Au substrate.

Ellipsometric measurements were performed on dry films in air using a Gaertner L2W26D ellipsometer, 70° angle of incidence, 633 nm wavelength. For monolayer films the index of refraction and the thickness cannot be determined independently,[39] so thickness is calculated based on an assumed index. Normally, an optical model consisting of a homogeneous thin film on a well characterized substrate is used for ellipsometric analysis, but in this case we know that the dendrimer films are inhomogeneous and therefore such a model is not appropriate. Instead, we employ an optical model of a composite film based on the Bruggeman effective medium approximation (EMA).[40] The index of refraction of the composite film is calculated based on the volume fractions and indices of

9

the individual film components. Single-component dendrimer films consist of dendrimer spheroids and void spaces, and two-component films consist of dendrimers, n-alkylthiol SAMs, and void spaces. The indices of the components are chosen to be 1.46 for dendrimers, 1.46 for the n-alkylthiols, and 1.00 for void spaces. The film thickness obtained from fitting this model to the ellipsometric measurements corresponds to the height of the dendrimer spheroids.

Advancing contact angles were measured in an ambient of the saturated vapor of the drop using a Ramé-Hart Model 100-00-115 goniometer. The drop size was about 2 mm. Data presented in the table were based on the average of at least three measurements performed on independently prepared films.

Gravimetric measurements were made using surface acoustic wave (SAW) mass balances at 25±0.5 °C using 2 ST-cut quartz oscillators housed in a custom-built flow system.[38,41] Modified SAW devices were dosed with volatile organic compounds (VOCs) diluted in N_2 to 25% of saturation (flow rate = 0.5 L/min). The change in SAW-device frequency (Δf) resulting from adsorption is related to the mass loading per unit area (m_a) through the equation $\Delta f/f_o = -\kappa c_m f_o m_a$. Here, f_o is the SAW resonance frequency (97 MHz), κ is the fraction of the center-to-center distance between the transducers covered by the Au film (in the present case its value is 0.7), and c_m is the mass sensitivity coefficient of the device (1.33 $cm^2/(g \cdot MHz)$ for ST-cut quartz).[41]

Most cyclic voltammetric and ac-impedance measurements were performed in a five-neck, three-electrode cell employing a Ag/AgCl (3 M NaCl) reference electrode (Bioanalytical Systems, West Lafayette, IN) and a Pt-gauze counter electrode, which was separated from the main compartment by a porous glass plug. The working electrode was cut from a Au-coated Si(100) wafer and contained within a Teflon O-ring holder that exposed an area of 0.09 ± 0.009 cm^2. All cyclic voltammetric measurements were carried out using a BAS Model 100B electrochemical analyzer (Bioanalytical System, Inc.). Impedance measurements were performed using an EG&G PARC 273A potentiostat and a Solartron 1255 frequency response analyzer controlled by a microcomputer running ZPLOT software (Scribner Associates, Charlottesille, VA). Measurements were performed using a 5 mV rms wave about E° of the Fe(CN)$_6^{4-/3-}$ redox couple, and impedance values were determined at five discrete frequencies per decade. The range of frequencies applied was 0.1 Hz to 65 kHz.

The charge-transfer resistance R_{ct} and the total capacitance C_t,[42] which is equal to the sum of the film capacitance (C_f) and the double-layer capacitance (C_{dl}), and some parameters relative to the diffusion process can be obtained by fitting the experimental impedance data to Randles' equivalent circuit using ZSIM/CNLS software (Scribner Associates). The Randles' equivalent circuit, while not the only possible representation, has frequently been employed to represent modified electrochemical interfaces[42-44] and in the present case provided an excellent fit to the data. The

diffusion element in the Randles' equivalent circuit is represented by a constant-phase element.[45]

Results and Discussion

Single-Component Dendrimer Monolayers. Amine-terminated PAMAM dendrimer monolayers are easily prepared by immersing a Au substrate in a dilute ethanolic solution of the dendrimer for 15-20 h and then rinsing with ethanol and water. Part a of Figure 1 shows an FTIR-external reflection spectroscopy (FTIR-ERS) spectrum of a G4 PAMAM monolayer. The relevant peaks confirming attachment of the dendrimer to the surface arise from the dendrimer framework: the amide I and amide II bands at 1665 and 1555 cm^{-1}, respectively, and bands resulting from the two kinds of methylene groups present in PAMAM dendrimers at 2926, 2854, and 2818 cm^{-1}, and the amide and amine N-H stretching modes centered around 3300 cm^{-1}.[46] The magnitude of the amide peaks is similar to that found for dendrimer monolayers covalently linked to Au surfaces via an intermediate *n*-alkylthiol monolayer.[4] The dendrimer monolayer is sufficiently stable so that sonication in ethanol or water for 5 min, exposure to quiescent ethanol for up to 24 h, or exposure to a pH 11 aqueous buffer solution for 15 h does not cause any change in the FTIR-ERS spectrum or ellipsometric thickness of the monolayer. However, exposure to a pH 2 aqueous buffer solution results in protonation of the amine groups and after 15 h results in about a 25% decrease in the amide peak area.

12

Figure 1

In contrast to this level of stability, we previously reported that simple primary alkylamines, which form SAMs on Au upon exposure to the corresponding vapor, are not stable under any of the aforementioned conditions.[47] The enhanced stability of dendrimer monolayers can be accounted for by two factors. First, the G4 dendrimer has a high surface area and a dense exterior, which, like linear polymers, results in a strong van der Waals interaction with the Au surface. Second, and most importantly, there are a large number of amine groups that chemisorb to the Au surface, and by analogy to polydentate metal-ion ligand chemistry, stabilize the amine/Au interaction. We have observed a similar phenomenon for thiol-terminated, polymerizable diacetylenic SAMs: prior to polymerization each molecule interacts with the substrate only through one thiol/Au chemical interaction, but after polymerization the stability of the polypodal polymer chains is greatly enhanced.[48] The importance of the Au/amine interaction is confirmed by carrying out the deposition at different pH values in aqueous solutions. When the deposition is performed at pH 2 the amide peak area arising from dendrimers in the resulting film amounts to about 25% of that observed when the deposition takes place in pure ethanol. At pH 11 this value increases to about 80%. We interpret this result in terms of the acid/base behavior of the terminal amine groups: at pH 2 they are protonated (pK_a about 9.5),[49] which ties up the lone pair of electrons on the terminal primary amines and reduces the strength of the Au/amine

13

interaction, but at pH 11 the lone pair is available to engage the Au substrate.

Higher and lower generation dendrimers also form monolayers on Au substrates. Figure 2 compares FTIR-ERS spectra of the amide region for G0, G2, G4, and G8 PAMAM dendrimers; even the G0 dendrimer, which has just four terminal amine groups, yields a significant coverage as judged by the amide peak intensities.

Figure 2

To quantify the dendrimer coverages, we used a mass-titration method that relies on surface-acoustic wave (SAW) mass balances. We have previously shown that when a Au surface is dosed with vapor-phase $CH_3(CH_2)_6SH$ (C7SH) a mass corresponding to a single monolayer adsorbs.[50] Additionally, we have demonstrated that if there are objects on the surface blocking adsorption sites, this method can be used to determine the number of unblocked sites.[51] Therefore, it is possible to determine the fractional surface coverage of dendrimers quantitatively by dosing a dendrimer-modified Au surface with vapor-phase C7SH and comparing the resulting mass change to that observed on a naked Au substrate.

When a SAW device having a naked-Au surface is dosed with dilute C7SH vapor, an average frequency change of ~10 ppm is observed, which corresponds to a surface coverage of 0.96 nmol/cm^2. The calculated maximum coverage of C7SH on a perfect Au(111) crystal is 0.78 nmol/cm^2. The ratio of these two values, 1.2,

agrees with our previous results and corresponds to the surface roughness of the electron-beam deposited Au films used in this study.[36,38] When the SAW devices are modified with a G4 PAMAM dendrimer monolayer prior to dosing, a C7SH coverage of 0.12 ± 0.02 nmol/cm^2 is measured. Comparison of this value to that obtained on the naked Au surface indicates that 88% of the Au surface is blocked by the dendrimer (Table 1). This experimentally determined value can be compared to the calculated maximum dendrimer surface coverage: assuming a hexagonal close-packed array of spherical G4 dendrimers, the projected surface coverage is about 91%. Thus, within the bounds of these approximations, the G4 dendrimer coverage of the Au surface is within 97% of the theoretical maximum. Accordingly, we feel comfortable describing these surfaces as true SAMs.

Table 1

Coverages for the G0-G8 dendrimers are given in Table 1. The G8 coverage (76%) is somewhat lower than G4 (88%). This probably reflects reduced surface mobility and a reduction in the reversibility of dendrimer sorption for the larger dendrimers, which is a consequence of the much greater contact area and number of amine groups on the exterior of the larger dendrimer (1024 for G8, 64 for G4). The calculated coverages for G0 and G2 are 89% and 97%, respectively. Both of these molecules are flat, however, and thus the spherical-shape approximation does not strictly apply.[25] It should be emphasized that these coverages only reflect

the percentages of the Au surface masked by dendrimers and not their surface concentration. This is important because although the surface coverage of a G4 SAM prepared at room temperature or at 50 °C is almost the same (Table 1), the surface concentrations are different. As discussed later, this is a consequence of the flexible dendrimer structure.[25]

Part a of Figure 3 shows the relationship between dendrimer concentration, as gauged by the sum of the amide I and II peak areas (Figure 2 and Table 1) normalized to that of G0, as a function of the bulk-phase dendrimer diameter[49] for the different generations (filled circles). As the generation increases, the amide peak intensity increases. The open squares in this figure are calculated from geometric considerations for the G0-normalized amide I plus II peak areas assuming adsorption of a perfectly spherical, hexagonal close-packed array of dendrimers. Clearly there is a significant deviation of the theoretical expectation of this model from that measured spectroscopically (filled circles). This deviation is especially apparent for the G8 dendrimer. The low measured value could indicate that there is much less dendrimer on the surface than expected based on the simple theoretical packing model. However, we know from the mass titration that nearly 80% of the surface is covered with G8. Taken together, these data suggest that the dendrimer is not spherical, but rather compressed against the Au surface in an oblate configuration.[4] This results in a larger-than-expected dendrimer footprint and a correspondingly lower total number of amide bonds. The physical explanation for this result is that

interactions develop between the dendrimer and Au surface until they are balanced by the energy cost required for further mechanical distortion of the dendrimer. We will return to this important point later.

Figure 3

The dendrimer thickness is calculated from the ellipsometric measurements using an EMA model of a close-packed lattice of oblate dendrimer spheroids as shown at the top of Scheme 2. The results are given in Table 1 and plotted as a function of the diameter of the bulk dendrimer molecules in Figure 3b. The dendrimer thickness, d_0, is significantly smaller than the bulk-phase diameter, suggesting substantial distortion of the dendrimer on the surface. Assuming constant volume of the dendrimer molecules, this flattening of the spheroids results in larger spacing between dendrimers, $2r_0$, and a lower surface concentration than the theoretical maximum expected for a close-packed lattice of spherical dendrimers. For the G4 and G8 dendrimers, the surface concentration is estimated to be 62% and 45% of the theoretical maximum, respectively, which is in reasonable agreement with the FTIR-ERS results shown in Figure 3a.

Scheme 2

Note that the G4 dendrimer deposited at elevated temperature (50 °C) exhibits a higher density of amide groups (filled triangle,

Figure 3a), but a similar surface coverage of dendrimers (Table 1). This suggests less distortion and a higher surface concentration of the dendrimers. This is also born out by the ellipsometric measurements, which reveal a significantly larger dendrimer thickness, indicating less distortion of the molecule upon adsorption at higher temperature.

A computer-based simulation of dendrimer surface adsorption has recently been reported.[52] It describes the dendrimer adsorption geometry and the interaction energy between the dendrimer and the surface for G1-G8 dendrimers. The results indicate that higher generation dendrimers, G4 and G8 in our study, flatten and spread on the surface, while the lower-generation, G1 and G2 dendrimers adsorb weakly and retain their bulk-phase conformation. Our experimental results are in good agreement with these calculations.

Table 1 shows the advancing and receding contact angle of water on the four amine terminated dendrimer SAMs. All the contact angles are the same within experimental error, indicating similar dendrimer surface coverages and chemical properties. These data are fully consistent with the FTIR-ERS data and SAW-device mass titrations.

To determine the barrier properties of dendrimer monolayers in aqueous electrolyte solutions we performed a complete impedance analysis. Figure 4 shows complex-impedance (Nyquist) plots at several frequencies for naked Au and G4- and G8-PAMAM dendrimer-modified electrodes in a pH 6.3-buffered solution containing 5 mM each of $Fe(CN)_6^{3-}$ and $Fe(CN)_6^{4-}$. Since the plot shapes are

characterized by a semicircle at high frequencies and a linear relationship at lower frequencies, Randles' equivalent circuit[53] can be used to interpret the results and Simulation/Complex Nonlinear Least Squares (SIM/CNLS) fitting (solid line) of the data (open circles) typically produces excellent agreement. Physical parameters extracted from the fitting routine are provided in Table 2. For naked Au (Figure 4a), a $45°$ line characteristic of Warburg diffusion[53] dominates almost the entire range of frequencies and there is only a barely discernible semicircle at high frequencies. The dominance of the Warburg impedance indicates that the redox reaction is diffusion-controlled over a broad frequency range. By analyzing the slope of Z_R vs. $\omega^{-1/2}$,[54] we can obtain the diffusion coefficient (D) for the redox couple: 7.1×10^{-6} cm^2/s, which is in good agreement with literature values.[55] Very similar results are obtained when the electrodes are coated with G4 and G8 dendrimers at room temperature.

Figure 4

Table 2

We estimated the effective fractional dendrimer surface coverage (θ) using eq 1[43] where R_{ct}^0 and R_{ct} are the charge-transfer resistance of the redox-probe molecule measured at a naked Au electrode and the coated electrode, respectively.

19

$$\theta = (R_{ct} - R_{ct}^0)/R_{ct} \qquad (1)$$

This equation is derived from a defect-based model that assumes a heterogeneous surface composed of a fractional area that fully blocks electron transfer (θ) and a fractional area that is completely accessible to the redox probe molecule ($1-\theta$). Although FTIR-ERS, ellipsometry, and mass-titration results prove that a high percentage of the Au surface is covered with dendrimers (about 88% and 76% for G4 and G8, respectively), the effective fractional surface coverages measured by this electrochemical method are only 4.5%, and 16% for G4- and G8-dendrimers, respectively. These results imply, and data discussed later confirm, that $Fe(CN)_6^{3-/4-}$ easily penetrate the surface-confined dendrimers as well as the interstices between them. The electrochemically measured surface coverage of G8 is reproducibly higher than G4 (although the mass-titration data indicate the opposite), because the former is significantly less penetrable. This is a consequence of a much more sterically crowded exterior of G8.[25] Because the effective dendrimer surface coverage is very small, the diffusion regions in Figures 4b and 4c exhibit Warburg impedances corresponding to semi-infinite linear diffusion (straight line with a slope of -1). Additionally, the same value of D is obtained for the dendrimer-coated surface and the naked Au

surfaces indicating that the resistance to diffusion for the dendrimer coatings is negligible.

Figure 4 also provides information about differences in the redox-probe blocking ability of dendrimer SAMs as a function of the film-deposition temperature. For the G4-covered electrode prepared at 50 $^{\circ}$C (Figure 4d), a larger-diameter semicircle (R_{ct} = 3.5 $\Omega \cdot cm^2$) accompanies the mass transfer-limited behavior at lower frequencies. As discussed previously, the FTIR-ERS and ellipsometry data (Table 1) suggest that an increase in the film-preparation temperature yields a higher surface concentration of dendrimers. The electrochemical data are in accord with this finding. Additionally, the dendrimers may aggregate and interpenetrate reducing the effective area accessible to the redox couple. However, even at elevated preparation temperature there is still a large fractional area of the dendrimer-modified electrode available for electron transfer.

In addition to the amine-terminated, PAMAM dendrimers, we have also demonstrated that dendrimers having different chemical compositions directly adsorb to naked Au surfaces. For example, using the same procedure as for the amine-terminated dendrimers, hydroxy-terminated G4 PAMAM dendrimers (G4-OH) also spontaneously adsorb to Au. The FTIR-ERS spectrum (part b of Figure 1) reveals amide I and II and methylene peaks of approximately the same magnitude and position as found for the amine-terminated G4 PAMAM dendrimer. The ellipsometric thickness of about 23 Å and the surface coverage measured by mass titration (92%) are also

approximately the same as for the amine-terminated dendrimer
monolayers (Table 1).

We also prepared and characterized dendrimer coatings
prepared from diaminobutane(propylamine)$_{64}$-based dendrimers
functionalized with ferrocene moieties (D$_{64}$-Fc).[31,32,37,56] NMR
results indicate 70% functionalization of the terminal amines,
resulting in an average of 45 ferrocenes per dendrimer.
Electroactive dendrimer films were prepared by placing Au
substrates in 0.01 mM chloroform solutions of D$_{64}$-Fc. The presence
of the monolayers was confirmed by FTIR-ERS and ellipsometry, and
then the surfaces were characterized by cyclic voltammetry in
aqueous electrolyte solutions. The results (Figure 5) reveal the
voltammetry of a typical surface-confined layer: the anodic and
cathodic waves exhibit a peak splitting of 15 mV, and the full-
width at half maximum of the anodic wave is ~95 mV.[53] As has been
reported previously for ferrocene-modified dendrimers in bulk-
phases, these data indicate that the terminal ferrocene groups act
independently of one another.[37] The first-scan voltammogram shown
in Figure 5 reveals an asymmetry in the magnitudes of the
oxidation and reduction currents, indicating that the dendrimer
film is stable in the reduced state, but partially desorbs (after
just one voltammetric scan) upon oxidation to the more water-
soluble cationic form. By integrating the charge under the first
anodic wave, a surface coverage of ferrocene end groups of 8.4 x
10^{-10} mol/cm^2 is obtained. Assuming that all ferrocene units are
electroactive, and taking into account the average percentage

22

functionalization of each dendrimer, this yields a dendrimer coverage of 2×10^{-11} mol/cm^2. Previous theoretical calculations indicated a diameter of 5.2 nm for the ferrocene-modified dendrimers.[37] A hexagonal close-packed array of 5.2-nm spheroids yields a coverage of 7.4×10^{-12} mol/cm^2. Relative to this model, the experimentally determined surface coverage is 250% of a monolayer. This result suggests a significant distortion of the assumed spherical shape or perhaps the presence of more than one layer. The important point, however, is that dendrimers having different internal and external compositions adsorb to Au surfaces, which demonstrates the generality of this approach for preparing thin dendrimer films. Presumably dendrimers functionalized with other simple terminal groups, such as thiols or silanes, can be prepared for coating a broad range of substrate materials.

Figure 5

Mixed PAMAM Dendrimer/n-Alkylthiol Monolayers. Mixed monolayers of dendrimers and n-alkylthiols are easy to prepare and have some very interesting properties. The mixed SAMs are made by first preparing a dendrimer-only SAM as described in the previous section, and then soaking it in a dilute ethanolic solution of an appropriate n-alkylthiol for 15-20 h. Figure 1c shows an FTIR-ERS spectrum of a mixed monolayer consisting of G4 PAMAM dendrimers and C16SH (G4+C16SH) prepared in this way. There are two important points. First, there is no decrease in the amide I or

II bands, which originate exclusively from the internal amide groups of G4, compared to the initial dendrimer-only spectrum (Figure 1a), and in fact there is a slight increase in the amide I peak at around 1665 cm^{-1} (Table 1). This indicates that the presence of the co-adsorbed n-alkylthiol does not result in significant desorption of the G4 dendrimer, and the slight increase in the amide I band suggests an orientational change of the relevant dipoles.[57] Second, there is a significant increase of the peaks in the hydrocarbon stretching region (2800-3000 cm^{-1}) signaling the presence of a high fractional surface coverage of C16SH.

Referring to the spectrum shown in Figure 6b which is the difference of part a and c of Figure 1, we note that the peak positions and the relative peak ratios, but not intensities, of the asymmetric and symmetric CH_2 modes (2920 and 2851 cm^{-1}, respectively) are the same as for a C16SH-only monolayer (Figure 6a). This indicates that C16SH co-adsorbed with the dendrimer on the Au surface forms crystalline-like packing domains that are indistinguishable from a C16SH-only monolayer.[58] Moreover, on the basis of the relative intensities of the methyl peaks in the spectra of a single-component C16SH monolayer (Figure 6a) and the fractional C16SH coverage present in the mixed monolayer (Figure 6b), we estimate that about 60% of the Au surface area is occupied by C16SH in the mixed monolayer (we compare the methyl bands to avoid potentially overlapping alkyl and dendrimer methylene bands). Taken together with the SAW mass-titration data discussed

in the previous section, which indicated an dendrimer coverage of 88% prior to C16SH exposure, we conclude there is a very significant compression of the dendrimer footprint. Exposing the mixed monolayer to either a 1 mM ethanolic C16SH solution or pure ethanol for 6 additional days does not result in a significant change in either the FTIR-ERS spectra or the ellipsometric thickness, indicating a high level of stability.

Figure 6

In addition to the G4+C16SH mixed monolayers, we also prepared and characterized composite monolayers of G0, G2, and G8 with C16SH. FTIR-ERS spectra of the G0 and G2 dendrimer-containing surfaces reveal a decrease in the amide I and amide II peak intensities after thiol adsorption, while the amide-bond intensity associated with the G8 surface does not show any significant decrease (Table 1). This result indicates that the dendrimer surface on Au becomes more stable as the generation increases, which in turn strongly suggests that the strength of the dendrimer/Au interaction depends on the total number of amine/Au interactions per dendrimer. These results and conclusions are fully consistent with those discussed earlier for the dendrimer-only SAMs.

Contact angles measured for the dendrimer/thiol composites (Table 1) should be characteristic of the uppermost few angstroms of the surface.[59,60] For example, the G0-only interface has a contact angle of 33°, but this increases to 100° after

coadsorption of C16SH. This result indicates that the surface of the mixed SAM is dominated by C16SH, which is reasonable in view of the relative thicknesses of the G0-only (10 Å) and C16SH-only (21 Å) monolayer components. In contrast, the contact angle of the G8+C16SH surface is not much different from that of the G8-only surface, indicating that the hydrophilic primary amine groups of the dendrimer extend above the thiol component and dominate the surface characteristics.[61,62]

Ellipsometric measurements suggest a dramatic increase in thickness of the dendrimer SAMs after soaking in the C16SH solution. It is not possible to attribute this entire increase to the presence of a submonolayer coverage of C16SH. In other words, to account for the thickness increase it is necessary to invoke a conformational change in dendrimer geometry. To quantify the extent of dendrimer distortion we postulate the model shown in Scheme 2 and compare measured monolayer thicknesses before (d_0) and after (d_1) C16SH co-adsorption.

Initially, the monolayer consists only of the Au-supported dendrimer present as an oblate spheroid of height d_0 (values of d_0 are given in Table 1). After exposure to C16SH, however, the compressive force exerted on the dendrimers by C16SH causes them to assume a prolate configuration, which exposes additional Au surface sites for thiol co-adsorption. This two-component EMA optical model assumes the following: (1) the dendrimers can mechanically distort; (2) the concentration of dendrimer molecules on the surface, and the center-to-center distance between dendrimers, is the same before and after exposure to C16SH; (3)

the molecular volume of the dendrimers is constant (i.e., if the thickness, d_1, increases the radius, r_1, decreases; (4) the C16SH adsorbs to all exposed regions of the Au surface and the thickness of the C16SH SAM is 21 Å. Using this model, the dendrimer thickness in the mixed monolayers, d_1 (Table 1) is fit to the ellipsometric measurements. The ellipsometric analysis confirms the spectroscopic evidence discussed earlier that the adsorbed dendrimer changes from oblate to prolate. (In the case of G0 and G2, this distortion may actually be a reorientation of the semi-rigid, flat dendrimer to an upright rather than horizontal orientation with respect to the surface. In any case, the conclusions here apply most strictly to G4 and G8.) The fractional coverage of C16SH in the mixed monolayer films estimated from this model is about 75%, which is in good agreement with the semi-quantitative FTIR-ERS results shown in Figure 6b and support our contention that a dramatic distortion of the dendrimer occurs upon coadsorption of C16SH.

We expected that the extent of dendrimer distortion would be driven by a delicate balance between the relative energies of adsorption of the two monolayer components, the energy required to mechanically distort the dendrimer, and the energy gain associated with solvating the terminal amine groups of the dendrimers. Accordingly, it should be possible to distort the dendrimers to different extents by performing the co-adsorption step in different media. Parts c and d of Figure 6 show difference FTIR-ERS spectra for G4+C16SH mixed monolayers prepared by co-adsorption of the thiol component from vapor-phase N_2,[63] and liquid

hexane,[64] respectively, minus the initial G4-only monolayer.
Infrared spectra in the C-H region arising from the adsorbed C16SH
for both surfaces are quite similar; however, the peak intensities
are much smaller than when C16SH was co-adsorbed from ethanol
(Figure 6b). Correspondingly smaller changes in thickness and
contact angle are also observed. These results indicate that
hexane and N_2 are not good solvents for the dendrimers, and
therefore they are unable to assist the conformational change
illustrated in Scheme 2. Accordingly, the thiol component is
adsorbed only on the Au surface not initially shielded by the
dendrimer.

On the basis of the spectroscopic and ellipsometric evidence
provided so far, we propose the following mechanism for the rather
dramatic distortion of the dendrimers in the mixed dendrimer + n-
alkylthiol monolayers. In ethanol, the PAMAM dendrimer is
solvated and swollen by the polar solvent. This increased
solvation means that the interaction between the terminal groups
of the dendrimer and the Au surface is more open to competition
from other adsorbates.[47] During adsorption, C16SH competes with
the amine groups on the dendrimers for adsorption sites on the Au
surface. The degree of adsorption of the thiol is determined by
the balance between the energy loss due to the increased strain
within the dendrimers and loss of amine/Au adsorption interactions
versus the energy gain due to the adsorption of C16SH and the
increased solvation of the dendrimers. Eventually, no additional
amine groups can desorb because they are sealed within the thiol
fraction of the monolayer and thus can not be solvated by ethanol

(Scheme 1). To test this model, we next investigated the chemical properties and electrochemical behavior of these types of heterogeneous dendrimer surfaces.

To better understand the chemical properties of the single-component and mixed dendrimer interfaces, we performed gas-dosing experiments using a SAW device modified with a G4 dendrimer monolayer. The data in Figure 7a were obtained by exposing a G4-only modified SAW device to six volatile organic compounds (VOCs) present at 25% of saturation. Subsequently, and without removing the SAW device from the dosing cell, the monolayer was exposed to vapor-phase C7SH. This results in irreversible co-adsorption of a small amount of C7SH, but because there is no solvent present the conformation of the dendrimer does not change. Accordingly, there are only slight differences in the relative response of the VOCs before and after exposure to the vapor-phase thiol. Next, SAW devices were removed from the test fixture and soaked overnight in either a dilute ethanol or hexane solution of C16SH. Recall that the spectroscopic evidence described earlier (Figure 6 and Table 1) indicated that hexane is a poor solvent for the dendrimer and consequently little thiol co-adsorbs and the dendrimer distortion is negligible. Consistent with this picture, part c of Figure 7 again indicates only a small change in the SAW response to VOCs after soaking the devices in the C16SH/hexane solution. We conclude that the monolayer interface is not greatly changed from the initial G4-only condition after exposure to thiols present in the vapor phase or low-dielectric solvents. In contrast, however, when the SAW device is removed from the test fixture again and

exposed to an ethanolic C16SH solution large differences in the response of the interface to the six VOCs is observed (Figure 7d).

Figure 7

We propose that these results can be explained by dendrimer compression by the thiol as shown in Scheme 1. This conformational change affects the chemical properties of the organic interface and thus its chemical selectivity. Although largely speculation, we think it likely that the dendrimer interiors are less open in the compressed state, and that VOCs have more difficulty penetrating the dendrimer interiors, which results in an overall reduction in the amount of VOC adsorbed.[4,5] Additionally, a higher percentage of the Au surface is covered with the low-surface-energy n-alkylthiol when the dendrimers are compressed, which further reduces the extent of VOC adsorption.

Electrochemical data are also consistent with dendrimer compression upon thiol co-adsorption. Specifically, the fraction of the surface coated with the thiol is more efficient than the dendrimer at passivating the surface. Comparison of the impedance results for G4- and G8-modified electrodes before and after exposure to C16SH (parts b and e, and c and f of Figure 4, respectively) clearly indicate a decrease in the fraction of the electrode accessible to the $Fe(CN)_6^{3-/4-}$ redox couple, which is consistent with co-adsorbed C16SH. The fractional active area (1-θ) decreases from 0.96 and 0.84 for G4- and G8-dendrimer

monolayers, respectively, to 0.06 and 0.006 after exposure to C16SH, respectively (Table 2).

Closer examination of Figure 4 and Table 2 leads to another important conclusion: penetration of the mixed G4+C16SH surface by $Fe(CN)_6^{3-/4-}$ results primarily from intradendrimer mass transfer.[65] For example, the fractional active area $(1-\theta)$ for an Au electrode coated with C16SH only is about 100-fold smaller than the mixed G4+C16SH surface (part h of Figure 4 and Table 2). Obviously, the larger electroactive area is caused by the presence of the dendrimer. We hypothesize that redox-probe penetration occurs through the dendrimers, rather than at the vertical dendrimer/C16SH interface, because if the shear force exerted by the thiols is sufficient to deform the dendrimers, then surely it is sufficient to prevent penetration by $Fe(CN)_6^{3-/4-}$. To test this hypothesis we carried out several additional experiments.

Part f of Figure 4 shows the impedance data for the mixed G8+C16SH surface: the electrochemically active fraction is almost ten times smaller than for G4+C16SH. The interface between G8 and the thiols should be virtually identical to that of the G4 and the thiols, but the G8 has a more sterically crowded exterior. Accordingly, this steric crowding should hinder intradendrimer mass transfer for the G8 system, but not affect leakage at the dendrimer/thiol interface. This is exactly what we observe. It is also possible to calculate the diffusion coefficient for $Fe(CN)_6^{3-/4-}$ through the dendrimer-modified surfaces from the impedance data in Figure 4. The linear part of the impedance plot

31

for the G4+C16SH-modified surface is characteristic of Warburg impedance, indicating substantial overlap of the individual diffusion layers[45] on the dendrimer surface. The diffusion coefficient of $Fe(CN)_6^{3-/4-}$ at the G4+C16SH-coated electrode is 1.4 x 10^{-7} cm^2/s, which is 50 times smaller than that calculated for naked Au, but 100 times larger than that estimated for the G8+C16SH-modified surface.

To control the surface concentration of dendrimers in mixed monolayers, we prepared modified surfaces by competitive adsorption in solutions containing C16SH and G4 present at different ratios. FTIR-ERS results (not shown) reveal that the intensities of amide I and II bands increase as the ratio of G4:C16SH increases. Electrochemical measurements confirm this finding. Figure 8 shows cyclic voltammetry that arises from G4+C16SH-modified surfaces prepared by competitive co-adsorption of dendrimers and C16SH present in the following ratios (G4:C16SH): 1:1, 1:5, 1:10. Data are also included for an electrode modified by sequential adsorption of first dendrimer and then C16SH. The sequentially prepared mixed monolayer yields the highest current and a peak-shaped voltammogram indicating facile penetration of the interface by $Fe(CN)_6^{3-}$ (Figure 8). We interpret this result as being characteristic of a high concentration of dendrimer in the monolayer. However, for the surfaces prepared by simultaneous co-adsorption of dendrimer and thiol, the peak current decreases as the ratio of dendrimer in the soaking solution decreases. At a G4:C16SH ratio of 1:10 very little

current is observed indicating a small fraction of dendrimers in the monolayer.

Figure 8

We also obtained a voltammogram of $Ru(NH_3)_6^{3+}$ at a G4+C16SH-modified surface prepared by soaking the Au electrode in a 0.1 mM G4 plus 0.5 mM C16SH ethanolic solution. Interestingly, the current resulting from $Ru(NH_3)_6^{3+}$ reduction at the mixed monolayer surface is much smaller than that of $Fe(CN)_6^{3-}$ measured on exactly the same modified electrode. The results for the mixed monolayer-coated electrodes prepared in solutions of different dendrimer:C16SH ratios are essentially identical to the one shown in Figure 8. These data suggest that at low pH (pH=6.3 in this experiment) the amine terminal groups of the dendrimer are protonated and electrostatically block penetration, and hence electrochemical reduction, of the positively charged $Ru(NH_3)_6^{3+}$. This result confirms that dendrimers in the mixed monolayers permit selective intradendrimer mass and electron transfer.[65]

It is also possible to control the surface concentration of the PAMAM dendrimers electrochemically. Figure 9 shows FTIR-ERS data for an initially G4-only PAMAM dendrimer surface after scanning between -0.5 and +0.5 V at 20 mV/s in a 0.5 M KOH ethanolic solution containing 10 mM C5SH for up to 30 min. The spectra indicate that the amide bands associated with the dendrimers (1665 and 1555 cm^{-1}) decrease while the bands associated

33

with the C-H stretching modes of C5SH (2966 cm^{-1}) gradually increase as a function of the scan time. After 30 min, the data indicate that the dendrimer is completely replaced by the thiol. This means that the dendrimer can be electrochemically desorbed and thus its surface concentration tightly controlled using simple voltammetry.[66]

Figure 9

On-surface functionalization of dendrimer surfaces. Only dendrimers having termini functionalized with groups capable of a fairly strong chemical interaction with a particular substrate form stable monolayers. However, for particular applications it may be desirable to prepare dendrimers having one set of functional groups for anchoring the dendrimer to a surface and another set, on the other side of the dendrimer, for performing a specific function. While it is possible to prepare such materials using a convergent synthetic approach,[67] we have found it much easier to first immobilize the dendrimers and then functionalize only those terminal groups not involved in the surface interaction. Here we describe this strategy and demonstrate that dendrimer monolayers are sufficiently stable to survive on-surface functionalization.

We have discovered a number of different chemistries that are appropriate for linking functional groups to amine- and hydroxy-terminated dendrimer monolayers. Reactions of acid chlorides with amine-terminated dendrimers are among the most versatile class of

34

reactions we have studied. For example, a 4-(trifluoromethyl)benzoyl-functionalized G4 dendrimer (G4-F) can be prepared by soaking an amine-terminated, G4 monolayer of the type described earlier for 2 h in a 0.1 M DMF solution of 4-(trifluoromethyl)benzoyl chloride containing triethylamine. Figure 1d shows an FTIR-ERS spectrum of a G4-F monolayer prepared in this way and then subsequently soaked in a C16SH solution (G4-F+C16SH) to enhance surface stability. Prior to on-surface functionalization, the spectrum of the monolayer was identical to that shown in Figure 1a, but afterwards a band at 1329 cm^{-1} signals the presence of $-CF_3$ groups. Additionally, there is a slight increase in the amide-band intensities, which arises from the new amide linkages between the fluorinated functional groups and the dendrimers, indicating that the synthetic procedure does not result in a significant level of dendrimer desorption. The bands in the high-energy region of the spectrum arise principally from the methyl and methylene groups of the co-adsorbed n-alkylthiol component of the monolayer.

We examined the electrochemical properties of G4-F+C16SH monolayer by performing an ac-impedance analysis (Figure 4g). The results indicate that R_{ct} is almost 25 times larger than that of the unfunctionalized G4+C16SH monolayer (Figure 4e). This is a consequence of increased steric crowding on the dendrimer surface, which hinders intradendrimer mass transfer, and an increase in the hydrophobicity of the fluorinated surface.

Summary and Conclusions

Dendrimers of many different generations terminated in amine
or hydroxy groups have the ability to form stable, densely packed
monolayers via polydentate interactions with Au surfaces.
Importantly, the shape of the higher-generation dendrimers changes
from spheroidal in the bulk to a compressed, oblate configuration
on the surface. The shape change is driven by a delicate energy
balance between the Au/amine interactions, solvation of primary
amines, and the energy required to distort the dendrimer.
Electrochemical impedance studies indicate that surface-confined
dendrimers are quite porous in their lower generations, but as
their surfaces become more sterically crowded they become slightly
better diffusion barriers. We also showed that following
immobilization, free dendrimer terminal groups can undergo on-
surface functionalization, which greatly expands the technological
implications for dendrimer monolayers.

Co-adsorption of C16SH with a dendrimer monolayer causes a
significant distortion of the dendrimer structure. Simple
calculations for the G4 PAMAM surface indicate a change in shape
from oblate to prolate. SAW-based gravimetry and ac-impedance
measurements support this model. Our experiments suggest that the
primary driving force for this change is terminal-group solvation
by suitable, polar solvents. Studies of the mixed monolayers also
confirm that redox probe molecules penetrate the dendrimers and
can undergo electron transfer within their interiors. The
concentration of dendrimers within mixed monolayers can be
controlled by competitive adsorption or selective electrochemical

desorption. Importantly, the conditions under which the single- and two-component monolayers are prepared greatly influence both the structure and stability of the monolayers. For example, monolayers prepared in very dilute dendrimer solutions (10^{-7} to 10^{-9} M) or for very short times (< 1 min) result in lower dendrimer coverages and reduced stability. This suggests that time-dependent aspects of the adsorption process, such as interdigitation of dendrimer branches, might greatly influence the chemical and physical properties of the monolayers. We are studying these phenomena at the present time and will report on the results shortly.

Our results suggest that dendrimer monolayers will be extremely useful for the manipulation of surface properties. Indeed, we have already shown they hold promise as chemically selective interfaces, adhesion layers for polymers and metals,[6] and microreactors for metal clusters.[68] Dendrimers can also be incorporated into thicker polymeric materials where we have shown them to act as permselective membranes[69] and corrosion passivation layers.[70] Finally, the structure and ion-transport function of the mixed dendrimer/n-alkylthiol monolayers is somewhat analogous to that of phospholipid/protein membranes and thus might serve as a crude model for fundamental studies of the latter.

37

References and Notes

(1)   Ulman, A. *An Introduction to Ultrathin Organic Films*; Academic Press: Boston, 1991.

(2)   Swalen, J. D.; Allara, D. L.; Andrade, J. D.; Chandross, E. A.; Garoff, S.; Israelachvili, J.; McCarthy, T. J.; Murray, R.; Pease, R. F.; Rabolt, J. F.; Wynne, K. J.; Yu, H. *Langmuir* **1987**, *3*, 932.

(3)   Finklea, H. O. *Electroanal. Chem.* **1996**, *19*, 109.

(4)   Wells, M.; Crooks, R. M. *J. Am. Chem. Soc.* **1996**, *118*, 3988.

(5)   Tokuhisa, H.; Crooks, R. M. *Langmuir* **1997**, *13*, 5608.

(6)   Baker, L. A.; Zamborini, F. P., manuscript in preparation.

(7)   Dubois, L. H.; Nuzzo, R. G. *Annu. Rev. Phys. Chem.* **1992**, *43*, 437, and references therein.

(8)   Laibinis, P. E.; Whitesides, G. M. *J. Am. Chem. Soc.* **1992**, *114*, 9022.

(9)   Zamborini, F. P.; Crooks, R. M. *Langmuir* **1997**, *13*, 122.

(10) Crooks, R. M.; Ricco, A. J. *Acc. Chem. Res.*, in press.

(11) Ricco, A. J.; Crooks, R. M.; Osbourn, G. O., submitted for publication in Acc. Chem. Res.

(12) Bain, C. D.; Whitesides, G. M. *J. Am. Chem. Soc.* **1988**, *110*, 3665.

(13) Chan, K. C.; Kim, T.; Schoer, J. K.; Crooks, R. M. *J. Am. Chem. Soc.* **1995**, *117*, 5875.

(14) Kumar, A.; Whitesides, G. M. *Appl. Phys. Lett.* **1993**, *63*, 2002.

(15) Finklea, H. O.; Snider, D. A.; Fedyk, J.; Sabatani, E.; Gafni, Y.; Rubinstein, I. *Langmuir* **1993**, *9*, 3660.

(16) Widrig, C. A.; Chung, C.; Porter, M. D. *J. Electroanal. Chem.* **1993**, *310*, 335.

(17) Walczak, M. M.; Popenoe, D. D.; Deinhammer, R. S.; Lamp, B. D.; Chung, C.; Porter, M. D. *Langmuir* **1991**, *7*, 2687.

(18) Weisshaar, D. E.; Walczak, M. M.; Porter, M. D. *Langmuir* **1993**, *9*, 323.

(19) Tarlov, M. J.; Newman, J. G. *Langmuir* **1992**, *8*, 1398.

(20) Scott, J. R.; Baker, L. S.; Everett, W. R.; Wilkins, C. L.; Fritsch, I. *Anal. Chem.* **1997**, *69*, 2636.

(21) Zhou, Y.; Bruening, M. L.; Bergbreiter, D. E.; Crooks, R. M.; Wells, M. *J. Am. Chem. Soc.* **1996**, *118*, 3773.

(22) Zhou, Y.; Bruening, M. L.; Liu, Y.; Crooks, R. M.; Bergbreiter, D. E. *Langmuir* **1996**, *12*, 5519.

(23) Sun, F.; Castner, D. G.; Mao, G.; Wang, W.; McKeown, P.; Grainger, D. W. *J. Am. Chem. Soc.* **1996**, *118*, 1856.

(24) Lenk, T. J.; Hallmark, V. M.; Rabolt, J. F.; Häussling, L.; Ringsdorf, H. *Macromolecules* **1993**, *26*, 1230.

(25) Tomalia, D. A.; Naylor, A. M.; Goddard, W. A. *Angew. Chem. Int. Ed. Engl.* **1990**, *29*, 138, and references therein.

(26) Fréchet, J. M. J. *Science* **1994**, *263*, 1710.

(27) Zeng, F.; Zimmerman, S. C. *Chem. Rev.* **1997**, *97*, 1681.

(28) Knapen, J. W. J.; Made, A. W. v. d.; Wilde, J. C. d.; Leeuwen, A. W. v.; Wijkens, P.; Grove, D. M.; Koten, G. v. *Nature* **1994**, *372*, 659.

(29) Jansen, J. F. G. A.; de Brabander-van den Berg, E. M. M.; Meijer, E. M. *Science* **1994**, *266*, 1226.

(30) Kukowska-Latallo, J. F.; Bielinska, A. N.; Johnson, J.; Spindler, R.; Tomalia, D. A.; Baker, J. R., Jr., *Proc. Natl. Acad. Sci. USA* **1996**, *93*, 4897.

(31) Alonso, B.; Morán, M.; Casado, C. M.; Lobete, F.; Losada, J.; Cuadrado, I. *Chem. Mater.* **1995**, 7, 1440.

(32) Takada, K.; Díaz, D. J.; Abruña, H. D.; Cuadrado, I.; Casado, C.; Alonso, B.; Morán, M.; Losada, J. *J. Am. Chem. Soc.* **1997**, *119*, 10763.

(33) Watanabe, S.; Regen, S. L. *J. Am. Chem. Soc.* **1994**, *116*, 8855.

(34) Tsukruk, V. V.; Rinderspacher, F.; Bliznyuk, V. N. *Langmuir* **1997**, *13*, 2171.

(35) Saville, P. M.; Reynolds, P. A.; White, J. W.; Hawker, C. J.; Fréchet, J. M. J.; Wooley, K. L.; Penfold, J.; Webster, J. R. P. *J. Phys. Chem.* **1995**, *99*, 8283.

(36) Wells, M.; Dermody, D. L.; Yang, H. C.; Kim, T.; Crooks, R. M.; Ricco, A. J. *Langmuir* **1996**, *12*, 1989.

(37) Cuadrado, I.; Morán, M.; Casado, C. M.; Alonso, B.; Lobete, F.; García, B.; Ibisate, M.; Losada, J. *Organometallics* **1996**, *15*, 5278.

(38) Yang, H. C.; Dermody, D. L.; Xu, C.; Ricco, A. J.; Crooks, R. M. *Langmuir* **1996**, *12*, 726.

(39) Tompkins, H. A. *A Users Guide to Ellipsometry*; Academic: New York, 1993; Vol. Apendix B.

(40) Aspnes, D. E.; Theeten, J. B.; Hottier, F. *Phys. Rev. B* **1979**, *20*, 3292.

(41) Ricco, A. J. *The Electrochem. Soc. Interface* **1994**, *3*, 38.

(42) Zhao, M.; Zhou, Y.; Bruening, M. L.; Bergbreiter, D. E.; Crooks, R. M. *Langmuir* **1997**, *13*, 1388.

(43) Sabatani, E.; Rubinstein, I. *J. Phys. Chem.* **1987**, *91*, 6663.

(44) Sabatani, E.; Cohen-Boulakia, J.; Bruening, M.; Rubinstein, I. *Langmuir* **1993**, *9*, 2974.

(45) Bottelberghs, P. H.; Broers, G. H. J. *J. Electroanal. Chem.* **1976**, *67*, 155.

(46) Lin-Vien, D.; Colthup, N. B.; Fateley, W. G.; Grasseli, J. G. *Infrared and Raman Characteristic Frequencies of Organic Molecules*; Academic Press: San Diego, 1991.

(47) Xu, C.; Sun, L.; Kepley, L. J.; Crooks, R. M.; Ricco, A. J. *Anal. Chem.* **1993**, *65*, 2102.

(48) Kim, T.; Chan, K. C.; Crooks, R. M. *J. Am. Chem. Soc.* **1997**, *119*, 189.

(49) Technical data supplied by Dendritech, Inc. (Midland, MI).

(50) Thomas, R. C.; Sun, L.; Crooks, R. M.; Ricco, A. J. *Langmuir* **1991**, *7*, 620.

(51) Dermody, D. L.; Crooks, R. M.; Kim, T. *J. Am. Chem. Soc.* **1996**, *118*, 11912.

(52) Mansfield, M. L. *Polymer* **1996**, *37*, 3835.

(53) Bard, A. J.; Faulkner, L. R. *Electrochemical Methods: Fundamentals and Applications*; John Wiley & Sons, Inc.: New York, 1980, pp 718.

(54) Sluyters-Rehbach, M.; Sluyters, J. H. *In Electroanalytical Chemistry*; Marcel Dekker: New York, 1970; Vol. 4.

(55) Saji, T.; Yamada, T.; Aoyagui, S. *J. Electroanal. Chem.* **1975**, *61*, 147.

(56) Shu, C.-F.; Shen, H.-M. *J. Mater. Chem.* **1997**, 7, 47.

(57) Nuzzo, R. G.; Dubois, L. H.; Allara, D. L. *J. Am. Chem. Soc.* **1990**, *112*, 558.

(58) Bain, C. D.; Whitesides, G. M. *J. Am. Chem. Soc.* **1988**, *110*, 5897.

(59) Wilson, M. D.; Ferguson, G. S.; Whitesides, G. M. *J. Am. Chem. Soc.* **1990**, *112*, 1244.

(60) Bain, C. D.; Evall, J.; Whitesides, G. M. *J. Am. Chem. Soc.* **1989**, *111*, 7155.

(61) Drelich, J. *Polish J. Chem.* **1997**, *71*, 525.

(62) Bain, C. D.; Evall, J.; Whitesides, G. M. *J. Am. Chem. Soc.* **1989**, *111*, 7155.

(63) Thomas, R. C.; Sun, L.; Crooks, R. M.; Ricco, A. J. *Langmuir* **1991**, 7, 620.

(64) Zhao, M.; Tokuhisa, H.; Crooks, R. M. *Angew. Chem. Int. Ed. Engl.* **1997**, *36*, 2598.

(65) Weisshaar, D. E.; Lamp, B. D.; Porter, M. D. *J. Am. Chem. Soc.* **1992**, *114*, 5860.

(66) Hawker, C.; Fréchet, J. M. J. *J. Am. Chem. Soc.* **1990**, *112*, 7638.

(67) Zhao, M.; Sun, L.; Crooks, R. M., manuscript in preparation.

(68) Liu, Y.; Zhao, M.; Bergbreiter, D. E.; Crooks, R. M. *J. Am. Chem. Soc.* **1997**, *119*, 8720.

(69) Zhao, M.; Liu, Y.; Crooks, R. M.; Bergbreiter, D. E., maniscript in preparation.

Table 1. Thickness, amide I + II peak area, dendrimer coverage, and contact angle of Gn dendrimer and Gn/C16SH mixed monolayers.

	Gn Dendrimer Monolayer				Mixed Gn/C16SH Monolayer		
	thickness $(d_0, Å)$[d]	amide I+II peak area $(A \cdot cm^{-1})$	dendrimer coverage $(\%)$[c]	contact angle (degrees)	thickness $(d_1, Å)$[d]	amide I+II peak area $(A \cdot cm^{-1})$	contact angle (degrees)
G0 (4, 15 Å)[a]	10±1	0.15±0.04	89	33±2	32±3	0.08±0.03	100±2
G2 (16, 29 Å)	22±2	0.30±0.04	97	30±4	49±2	0.23±0.11	92±4
G4 (64, 45 Å)	28±2	0.37±0.04	88	32±3	53±2	0.34±0.06	80±12
50 °C	35±1	0.55±0.04	85	31±3	64±3	0.51±0.03	76±11
G8 (1028, 97 Å)	44±1	0.55±0.05	76	35±4	95±5	0.55±0.04	56±14
G4-OH[b]	23±2	0.32±0.06	92	23±2			

[a]Number of terminal groups and bulk-phase diameters measured in an aqueous acidic buffer solutions at pH = 2.7-3.0 determined by size exclusion chromatography using linear polymers (polyethylene glycol) as standards.[49] [b]Hydroxyl-terminated dendrimer. [c]Measured by mass titration (see text). [d]The distances d_0 and d_1 refer to the dimensions shown in scheme 2. All measurements were made on films prepared at 22±2 °C unless otherwise indicated.

Table 1/Tokuhisa et al.

Table 2. Average charge-transfer resistance (R_{ct}), apparent surface coverage (θ), fractional active area ($1-\theta$), interfacial capacitance (C), and diffusion coefficient (D) of naked Au and Au coated with dendrimer films in 5 mM $Fe(CN)_6^{3-}$ + 5 mM $Fe(CN)_6^{4-}$ (pH = 6.3, 0.5 M Na_2SO_4, at 22±2 °C). Results calculated from data presented in Figure 4.

electrode	$R_{ct}(\Omega.cm^2)$[a]	θ	$1-\theta$	C, $\mu F/cm^2$ [a]	D, cm^2/s [b]
Au	2.1	0	1	28	7.1×10^{-6}
Au/G4	2.2	0.045	0.955	24	7.1×10^{-6}
Au/G8	2.5	0.16	0.84	25	7.1×10^{-6}
Au/G4, 50°C	3.5	0.40	0.60	20	7.1×10^{-6}
Au/G4+C16SH	37	0.94	0.06	2.2	1.4×10^{-7}
Au/G8+C16SH	340	0.994	0.006	1.6	$\sim 1 \times 10^{-9}$
Au/G4-F+C16SH	820	0.997	0.003	1.8	-
Au/C16SH	2400	0.9992	0.0008	1.3	-

[a]R_{ct} and C were obtained by fitting the data to Randles' equivalent circuit using ZSIM software. The solution resistance was 97 Ω. [b]D was obtained by analyzing the slope of Z_R vs. $\omega^{-1/2}$.

Table 2/Tokuhisa et al.

Figure 1. FTIR-ERS of dendrimer surfaces. (a) Amine-terminated G4 PAMAM dendrimer monolayer; (b) Hydroxy-terminated G4 PAMAM dendrimer monolayer; (c) Mixed monolayer of PAMAM G4 dendrimer and C16SH; (d) Mixed monolayer of 4-(trifluoromethyl)benzamido-terminated G4 PAMAM dendrimer and C16SH.

Figure 2. FTIR-ERS of G0-G8 PAMAM dendrimer monolayers prepared on Au in the amide region.

Figure 3. (a) Plot of the sum of the amide I + amide II peak areas obtained from the spectra in Figure 2, normalized to G0 as a function of bulk-phase dendrimer diameter (filled circles, except G4 surface prepared at 50 °C which is represented as a filled triangle), and the G0-normalized amide number density calculated for a hexagonal close-packed monolayer of spherical PAMAM dendrimers (squares). (b) Plot of calculated ellipsometric thickness using the EMA for G0-G8 dendrimer monolayers vs. their bulk-phase diameters.

Figure 4. Complex impedance plots (open circles) at many frequencies (Hz) obtained from nominally naked Au, dendrimer monolayers (Au/Gn), and mixed dendrimer/C16SH monolayers in a pH 6.3 phosphate-buffered aqueous 0.5 M Na_2SO_4 solution containing 5 mM $Fe(CN)_6^{3-}$ and 5 mM $Fe(CN)_6^{4-}$. All the films were prepared and characterized at 22±2 °C except (d) which was prepared at 50 °C.

The continuous lines represent the ZSIM/Complex Nonlinear Least Squares (CNLS) fit calculated according to Randles' equivalent circuit. Electrode area: $0.09\pm0.009\,cm^2$.

Figure 5. The first cyclic voltammogram of diaminobutane-*dendri*-(propylamine)$_{64}$ (dashed line) and ferrocene-modified diaminobutane-*dendri*-(propylamine)$_{64}$ (solid line) monolayers adsorbed to a Au electrode. Scan rate = 100 mV/s, electrolyte solution: 1.0 M $HClO_4/H_2O$, electrode area: $0.09\pm0.009\ cm^2$.

Figure 6. FTIR-ERS in the CH_x stretching region (a) C16SH-only monolayer prepared by deposition from a ethanolic C16SH solution. Difference spectra obtained by subtracting a G4-only spectrum (Figure 1a) from the spectrum of a G4+C16SH surface prepared by thiol deposition from (b) a 1 mM ethanol solution of C16SH (Figure 1c); (c) saturated vapor of C16SH in N_2 at 40 °C, (d) a 1 mM hexane solution of C16SH.

Figure 7. Response of G4 PAMAM dendrimer-modified SAW devices to 6 VOCs. (a) Response of a SAW device modified only with G4 dendrimer. (b) Response of the device from part (a) after exposure to vapor-phase C7SH diluted with N_2. (c) Response of the device from part (b) after exposure to a 1 mM hexane solution of C16SH for 20 h. (d) Response of the device from part (b) after exposure to a 1 mM ethanolic solution of C16SH for 20 h. All

experiments were performed using 25%-of-saturation VOC. Responses

shown are from an average of at least 2 different devices.

Figure 8. Cyclic voltammetry of 5 mM $Fe(CN)_6^{3-}$ and $Ru(NH_3)_6^{3+}$ in

a 0.5 M Na_2SO_4, pH = 6.3 phosphate-buffered electrolyte solution.

(O) Electrode prepared by sequential adsorption from ethanolic

solutions of 0.1 mM G4 first then 1 mM C16SH. Electrodes prepared

by simultaneous adsorption from ethanolic solutions containing 0.1

mM G4 and (+) 0.1 mM C16SH, (Δ) 0.5 mM C16SH, (-) 1.0 mM C16SH.

For $Ru(NH_3)_6^{3+}$, only the data corresponding to (Δ) are shown; the

other three modified surface yielded results indistinguishable

from this. Electrode area: 0.09 ± 0.009 cm^2. Scan rate: 50 mV/s.

Figure 9. Time-dependent FTIR-ERS of a single dendrimer-modified

Au electrode illustrating electrochemical removal of dendrimers

and subsequent replacement by C5SH. The bottom spectrum was

obtained for a G4-coated electrode, and the remaining spectra were

obtained following electrochemical cycling (-0.5 to +0.5 V vs.

Ag/AgCl, 3 M NaCl) at 20 mV/s in a 10 mM ethanolic solution of

C5SH for the indicated time periods. The electrolyte was 0.5 M

KOH.

**Dendrimer-only
Monolayer**

Au

**Dendrimer + *n*-Alkylthiol
Mixed Monolayer**

Au

Au/PAMAM(G4)   Dendrimer   Void Space

d_0 r_0

Au

C16SH/EtOH

Au/PAMAM(G4)+C16SH   Void Space

Dendrimer

d_1 r_1
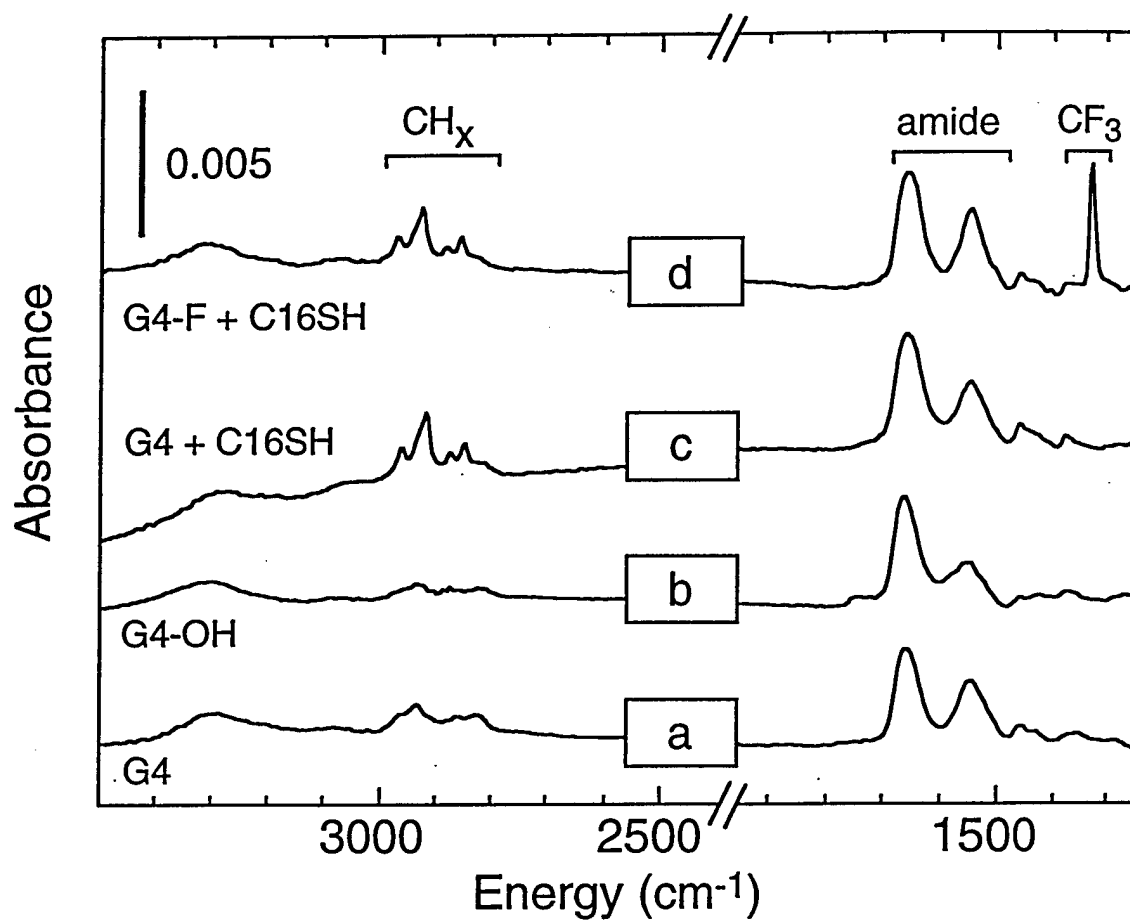
Au

C16SH
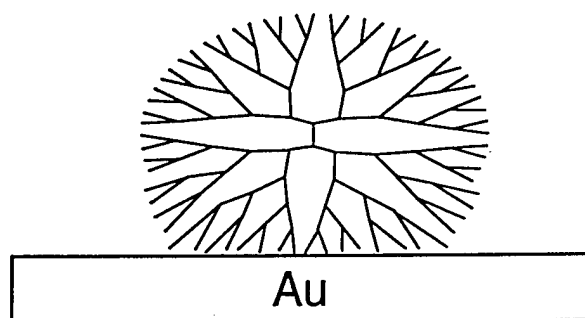
Scheme 2/Tokuhisa et al.
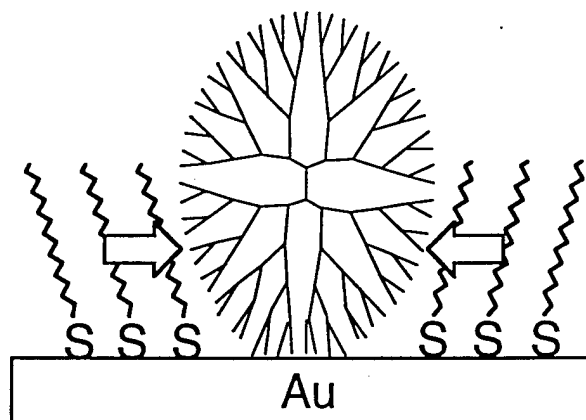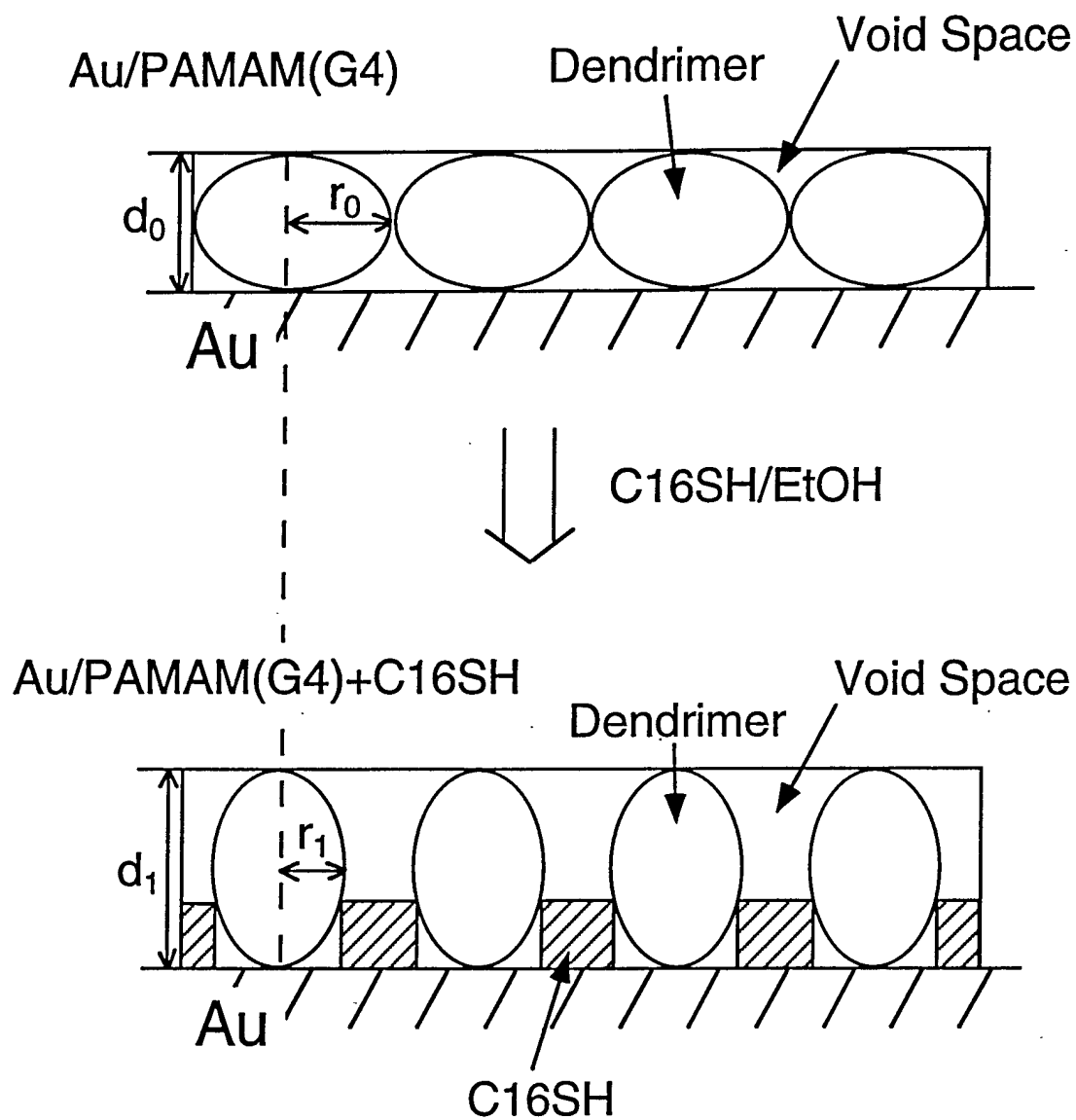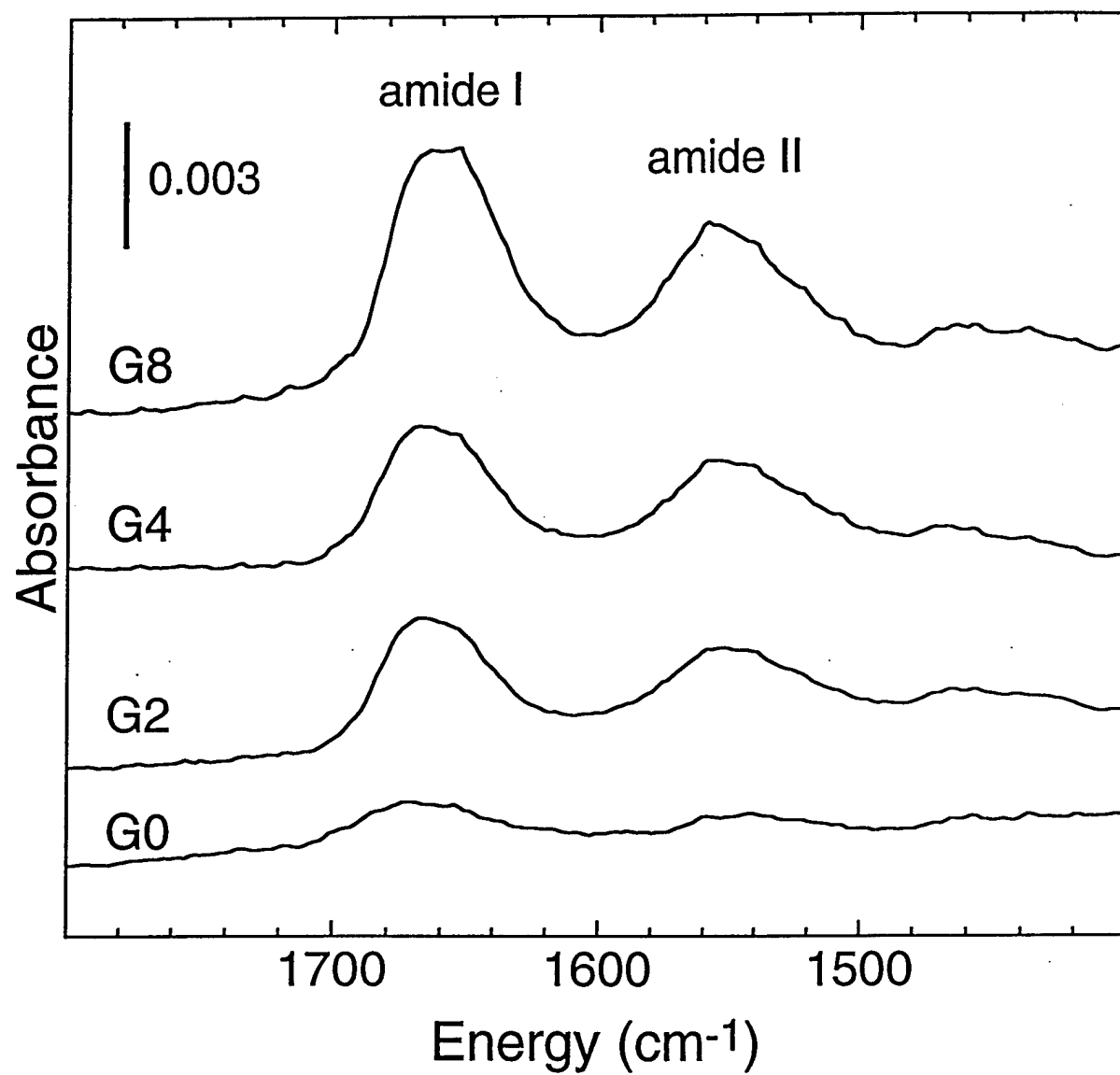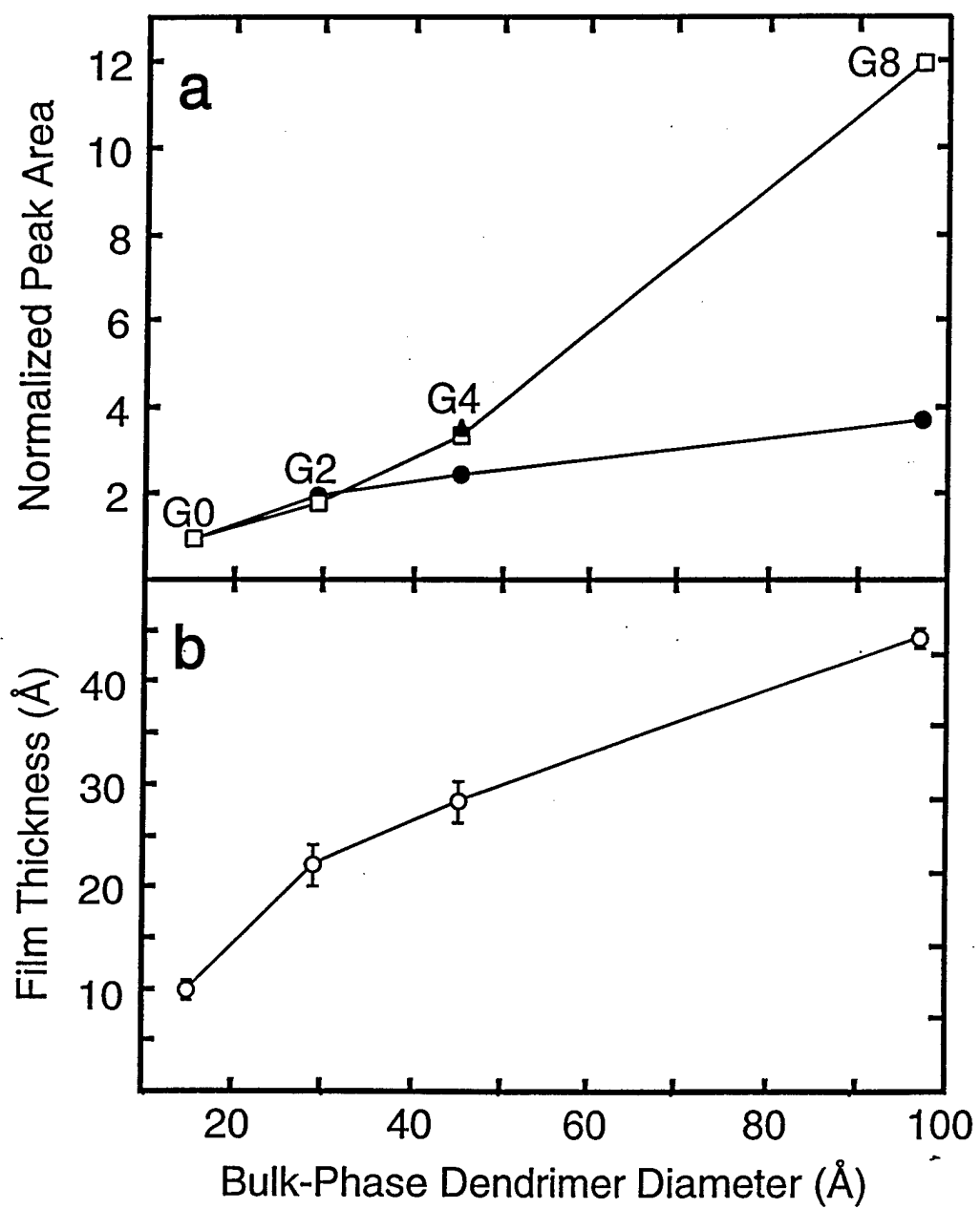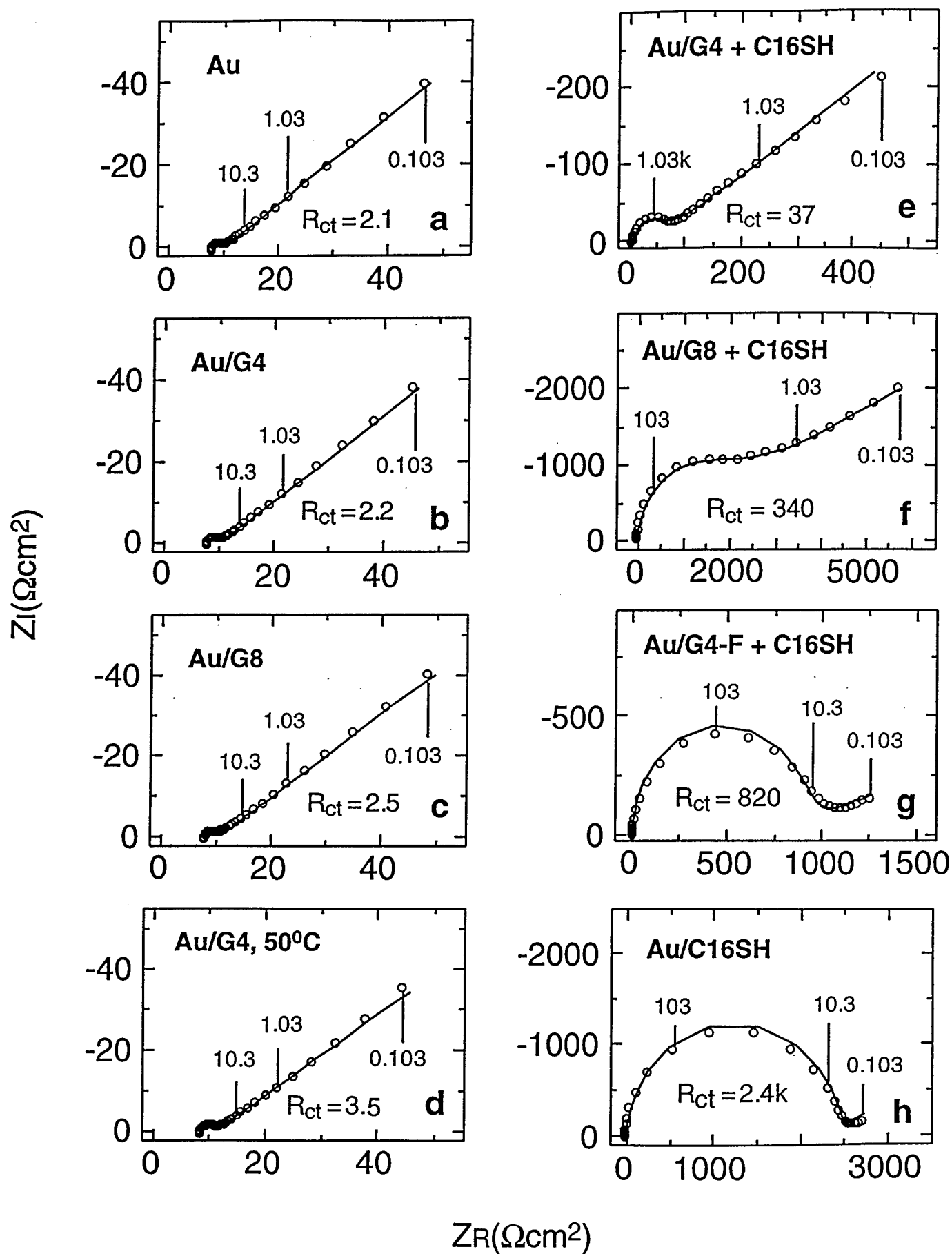
Figure 1/Tokuhisa et al.

Figure 2/Tokuhisa et al.
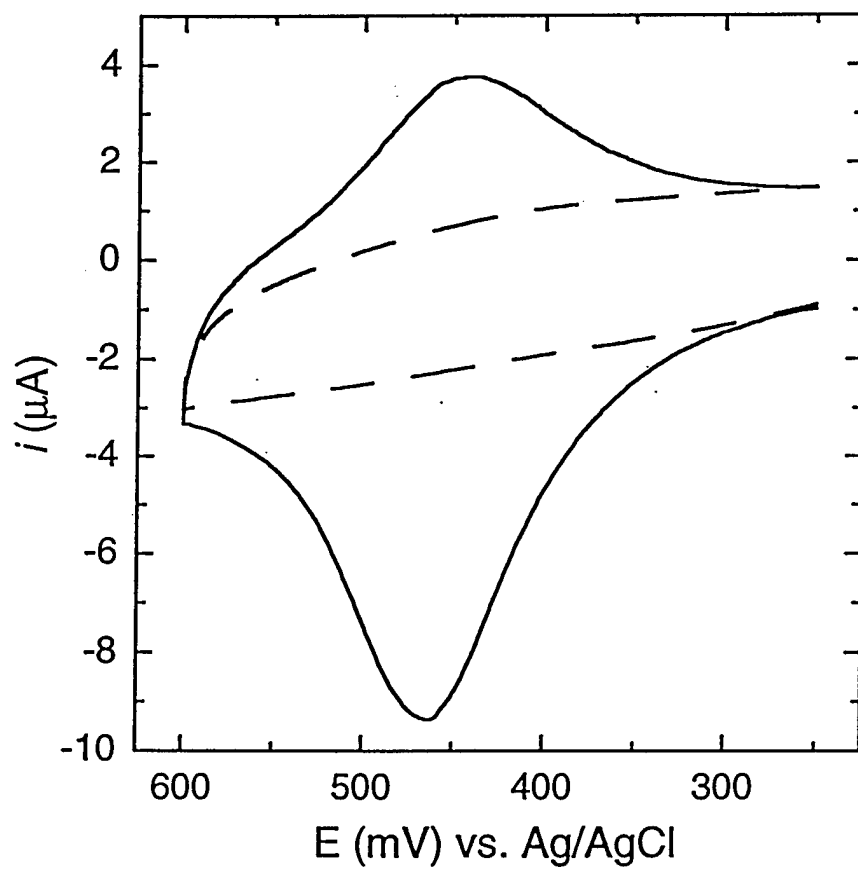
Figure 3/Tokuhisa et al.

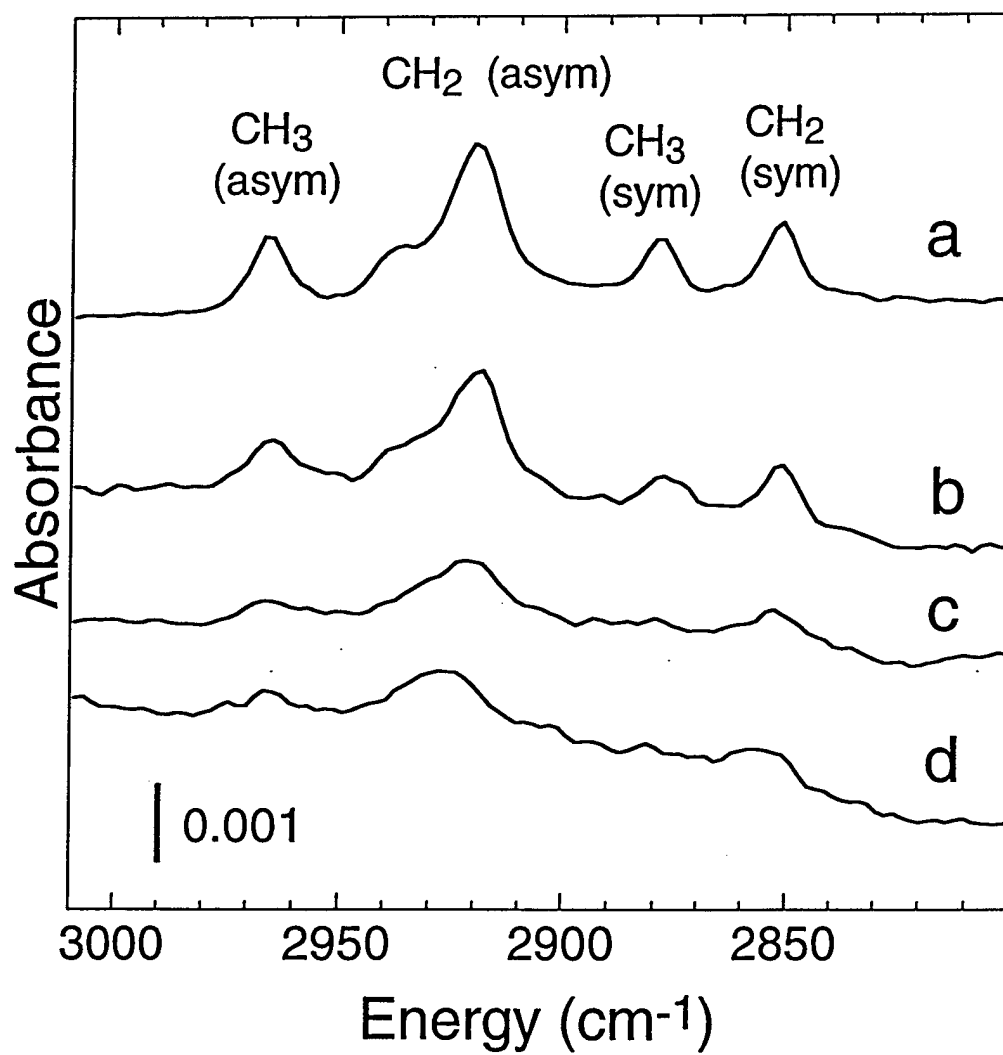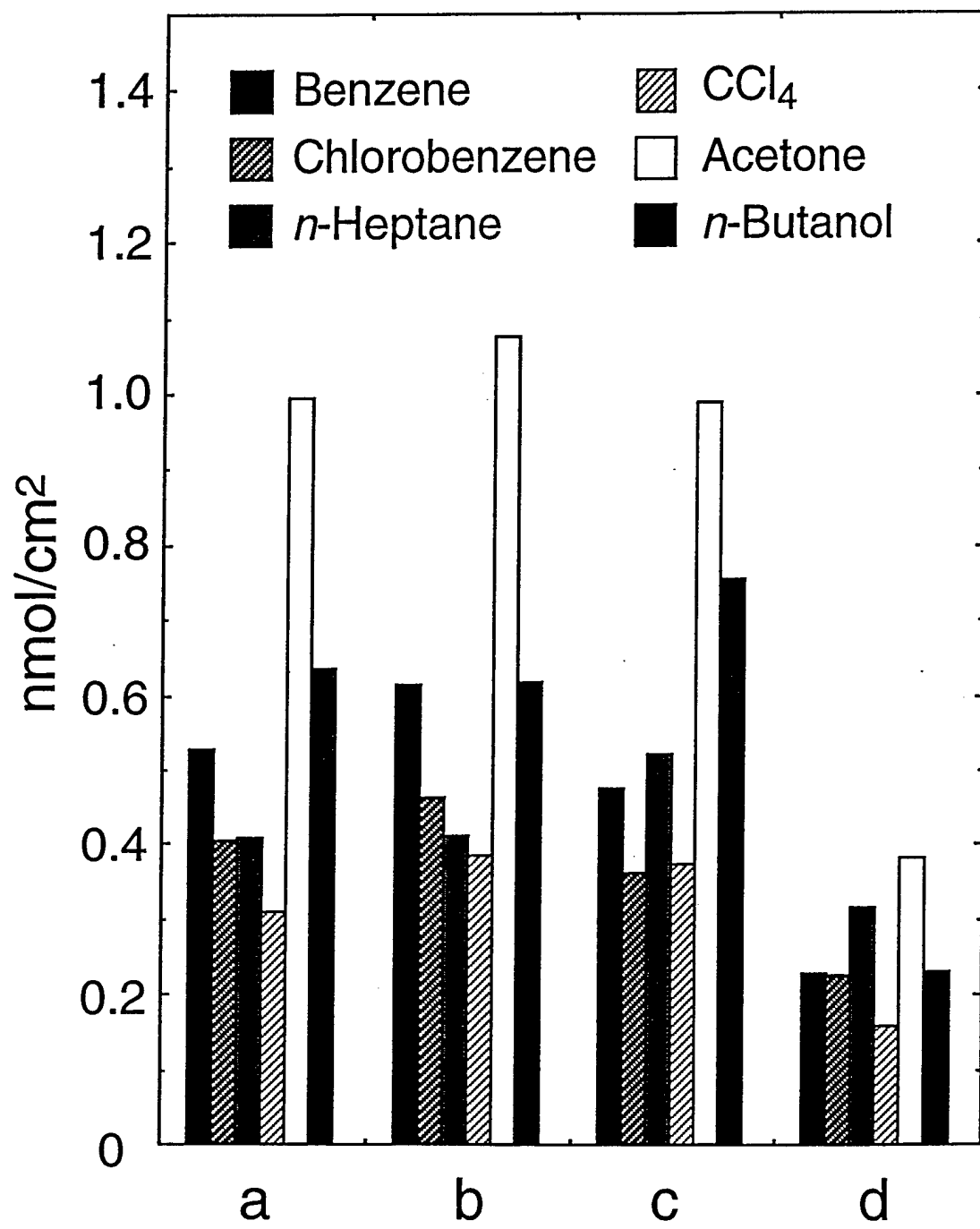Figure 4/ Tokuhisa et al.

Figure 5/Tokuhisa et al.

CH₂ (asym)

CH₃ (asym)

CH₃ (sym)

CH₂ (sym)

a

b

c

d

Absorbance

0.001

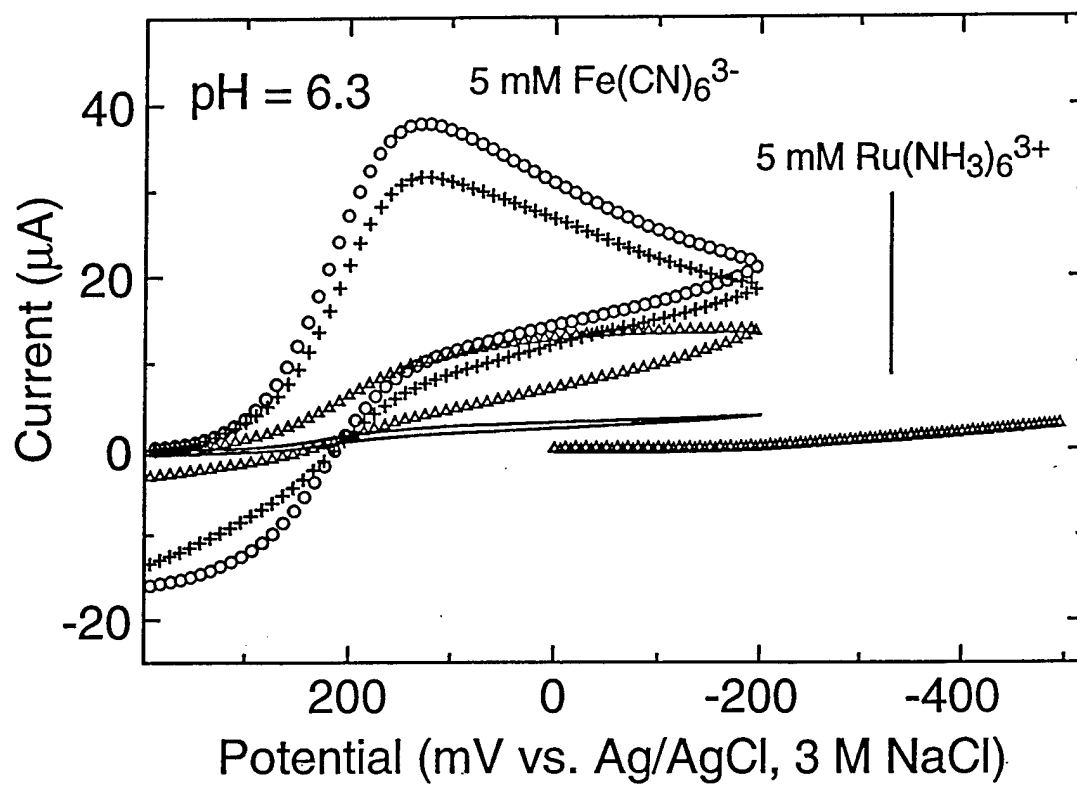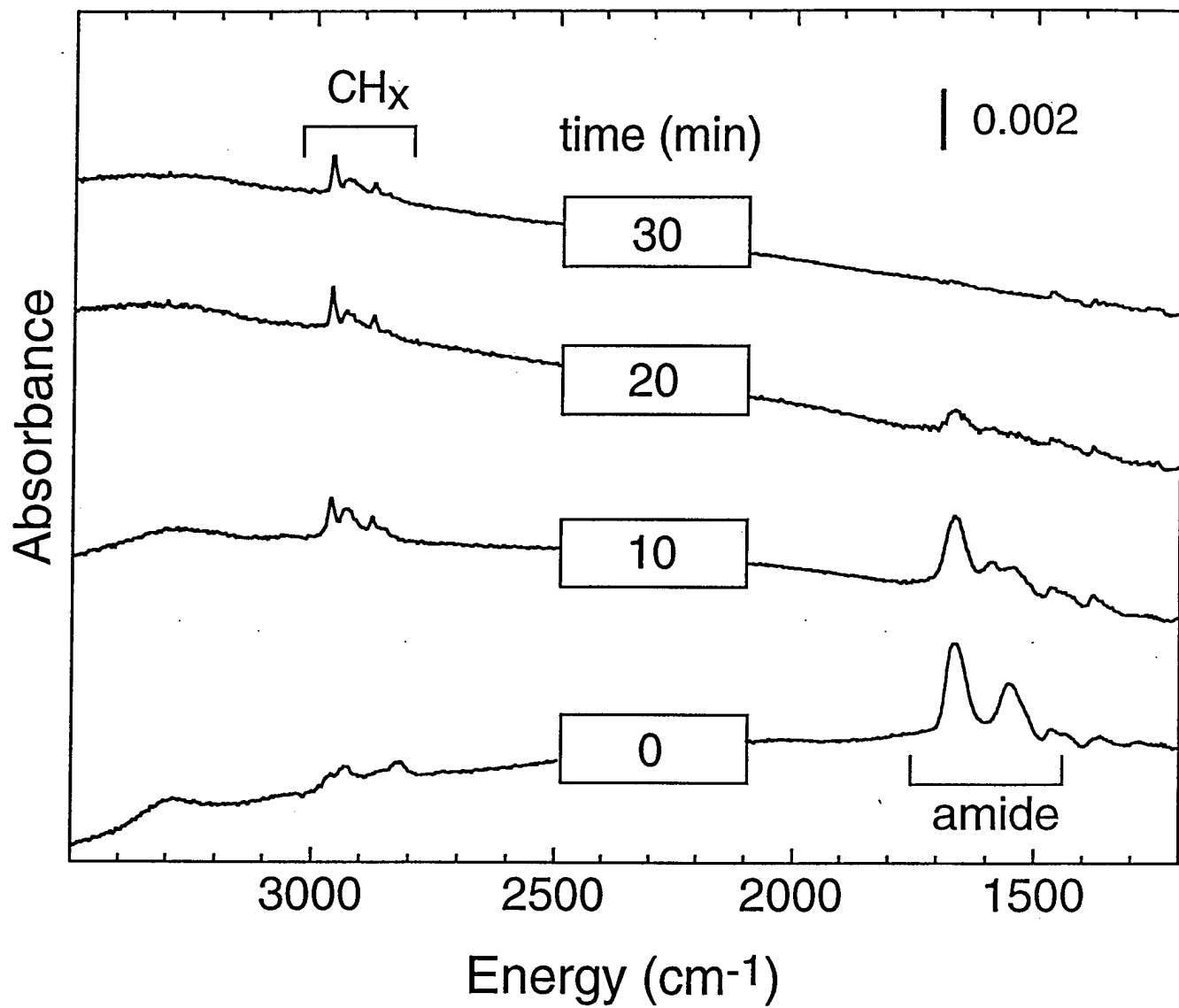3000   2950   2900   2850

Energy (cm⁻¹)

Figure 7/Tokuhisa et al.

Figure 8/Tokuhisa et al.

Figure 9/ Tokuhisa et al.